Gene Therapy (2010), 1–10

www.nature.com/gt

ORIGINAL ARTICLE

Improvement of lentiviral vector-mediated gene transduction by genetic engineering of the structural protein $Pr55^{Gag}$

T Aoki[1,2], S Shimizu[1], E Urano[1,3], Y Futahashi[1], M Hamatake[1], H Tamamura[2], K Terashima[4], T Murakami[1], N Yamamoto[1] and J Komano[1]

[1]*AIDS Research Center, National Institute of Infectious Diseases, Tokyo, Japan;* [2]*Department of Medicinal Chemistry, Institute of Biomaterials and Bioengineering, Tokyo Medical and Dental University, Tokyo, Japan;* [3]*Graduate School of Infection Control Sciences, Kitasato University, Tokyo, Japan and* [4]*Department of Comprehensive Pathology, Aging and Developmental Sciences, Tokyo Medical and Dental University, Graduate School, Tokyo, Japan*

The lentiviral vector is a promising tool for human gene therapy because of its ability to transduce genes into many cell types. However, one of the technical problems associated with the lentiviral vector is that lentiviral titers in current production systems are relatively low compared with the other viral vectors. In this study, we provide genetic evidence that the attachment of heterologous myristoylation (myr) signals on the amino-terminus of human immunodeficiency virus type 1 $Pr55^{Gag}$ (Gag) can increase the viral yield up to 10-fold, leading to the enhancement of gene transduction in many cell lines. The myr signal Gag constructs behaved similarly to the wild-type Gag in targeting to detergent-resistant membrane compartments, Vps4-dependence for viral budding, and virion morphology. However, the myr signal Gag constructs showed improved oligomerization efficiency as measured by bioluminescence resonance energy transfer in living cells, contributing to increased viral production and efficient activation of the viral protease responsible for virion maturation. The genetically modified Gag represents the next generation lentiviral vector, and should contribute to the success of many lentiviral vector applications.

Gene Therapy advance online publication, 22 April 2010; doi:10.1038/gt.2010.61

Keywords: *lentiviral vector; gag; myristoylation*

Introduction

The lentiviral vector is a powerful tool for transduction of genes into many cell types, especially non-dividing cells such as neurons, and is being used in clinical trials of human gene therapies and other applications.[1–8] The use of lentiviral vectors has been made possible because of advances in basic virology and because of a series of modifications that have increased the safety of the lentiviral vector. The commonly used third-generation lentiviral vector is a *Tat*-independent four-plasmid system composed of a gene transfer vector and three trans-vectors expressing Rev, Env and Gag-pol. The gene transfer vector is equipped with a self-inactivation LTR system (SIN). Viruses are often pseudotyped by vesicular stomatitis virus G (VSV-G). The human codon-optimized *gag-pol* expression vector is used to increase viral yield.[9]

The application of the lentiviral vector to human gene therapy was first approved for the treatment of human immunodeficiency virus (HIV) infections in the early 2000s.[1]. Since then, because of its potential advantages, the use of lentiviral vector has been expanding. A large amount of lentiviral particle must be produced for clinical trials. A technical improvement to increase the viral titer obtained from a production system would have a substantial effect on the cost of supporting a clinical human gene therapy trial using the lentiviral vector. The lentiviral vector titer in current production systems is generally in the order of 10^5–10^6 transducing units per ml. Although titer can be increased by centrifugation, the production yield is not as high as other viral vectors including the widely used adenoviral vectors. The HIV-1-based lentiviral vector has been engineered to reduce the risk of pathogenicity associated with HIV-1 [5,9], which resulted in a decrease of the viral titer.

Retroviral production and infectivity are regulated by the amino-terminal matrix domain ($p17^{MA}$ or MA) of $Pr55^{Gag}$ (Gag).[10–13] The myristoylation (myr) signal in the MA is critical for efficient viral production by aiding Gag trafficking to the plasma membrane (PM). In a previous study, we found that substitution of the HIV-1 Gag myr with the phospholipase C-δ1 pleckstrin homology (PH) domain increased the production of the third-generation lentiviral vector in which the *gag-pol* is human codon-optimized.[14] This prompted us to search for a PM-targeting signal that could enhance viral production to a greater extent than PH-Gag. Among the PM-targeting signals, we discovered that the myr signal motifs of

Correspondence: Dr J Komano, AIDS Research Center, National Institute of Infectious Diseases, 1-23-1 Toyama, Shinjuku, Tokyo, 162, Japan.
E-mail: ajkomano@nih.go.jp
Received 9 November 2009; revised 23 February 2010; accepted 7 March 2010

several heterologous proteins conferred such an effect. We suggest that the resulting modified Gag-based lentiviral vector can serve as a next generation lentiviral vector system, and should contribute to diverse applications of the lentiviral vector.

Results

We constructed HIV-1 Gag constructs (Figure 1a) containing the following PM-targeting proteins or PM-targeting signals fused to the Gag amino-terminus: the transmembrane proteins CD4, CD8, CXCR4, HIV-1 *Env*, or the acylation signal motifs of *lyn*, Gα(12), Gα(13) and Gα(16). This makes the original Gag myr signal unable to function. For CD4 and CXCR4, the full-length (FL) and cytoplasmic tail-deleted derivatives (DC) were examined. The membrane protein mutants are expected to traffic to the PM through the vesicular trafficking pathway involving ER and Golgi apparatus. As *lyn* encodes two overlapping acylation motifs, a myr and palmitoylation (pal) motif, we generated three *lyn*-derived constructs bearing a myr signal only, a pal signal only, or both signals (denoted myr^{lyn}, pal^{lyn}, myr/pal^{lyn}). In the *lyn* myr signal constructs, the position of the myristoyl group is –22 amino acids upstream from the original Gag context (denoted wild type, WT, hereafter). The *gag* and *env* sequences were human codon-optimized. The start codon and myr signal of Gag were destroyed by the M1L and G2A mutations to avoid internal translational initiation that could influence the experimental results.[14] The myr signal-defective Gag construct G2A was used as a negative control. PH-*gag* was used as a positive control that showed enhanced viral production.[14] The Gα(12), Gα(13) and Gα(16) constructs have one, two and three pal attachment sites, respectively. All the constructs were fused to green fluorescent protein (GFP), and expression was verified by western blot and immunoprecipitation analyses (Figure 1b).

A confocal microscopic analysis revealed that the majority of Gag-GFP was targeted to the PM, but some Gag-GFP was distributed in the cytoplasm with a fine vesicular pattern in 293FT cells (Figure 1c, WT). G2A-GFP showed a homogenous cytoplasmic distribution (Figure 1c). PH-Gag-GFP showed a distribution pattern similar to the WT (Figure 1c). These data are consistent with our previous findings.[14] The membrane protein Gag constructs mostly accumulated in the perinuclear region and only some of the protein was targeted to the PM, as verified by flow cytometric analysis using antibodies recognizing the extracellular domain of CD4, CD8 or CXCR4 (exemplified by the CXCR4^{FL} mutant in Figure 1c, and data not shown). The myr/pal^{lyn} construct showed a phenotype similar to WT with fine vesicular staining close to the nucleus (Figure 1c). The myr^{lyn} construct showed a PM-targeting phenotype similar to WT (Figure 1c). The pal^{lyn} construct was distributed evenly in the cytoplasm similar to G2A (Figure 1c). The Gα constructs were distributed predominantly in the cytoplasm with vesicular staining patterns, and less evidently at the PM (exemplified by the Gα(16) construct in Figure 1c).

To evaluate the efficiency of virus-like particle (VLP) production, we measured the GFP fluorescence intensity of culture supernatants containing VLP relative to the cell fraction (Figure 1d). PH-*gag* showed a significant enhancement of VLP production (229.0%, Figure 1d) compared with Gag-GFP, and the G2A construct produced almost no VLP, consistent with previous findings.[14] Membrane protein mutants produced little VLP (0.8–41.6% relative to Gag-GFP), presumably because they were inefficiently transported to the PM as evidenced by the confocal microscopy analysis (Figure 1c). Among the membrane protein mutants, CXCR4^{FL}-*gag*-GFP showed the best VLP production efficiency (41.6% relative to Gag-GFP). Interestingly, deleting the cytoplasmic tail of CXCR4 led to a drastic loss of VLP production (0.8% relative to Gag-GFP), suggesting that the cytoplasmic tail of CXCR4 somehow contributes to VLP production. Myr/pal^{lyn}-*gag*-GFP showed significantly greater VLP production than the WT (229.4%, $P<0.05$, Student's *t*-test). Myr^{lyn}-*gag*-GFP produced slightly more VLP than the WT (131.5%). Pal^{lyn}-*gag*-GFP showed a weak VLP production ability (14.1%), possibly because the pal signal did not function effectively, or the palmitoyl group did not function as a PM-targeting motif in the given protein context. The Gα(12)- and Gα(13)-*gag*-GFP constructs, containing one or two pal motifs, respectively, showed 7.0 and 7.3% VLP production efficiencies, compared with the WT. The Gα(16)-*gag*-GFP construct, containing three pal motifs, was able to produce VLP (28.8%) more effectively than the other Gα constructs, suggesting that the pal group serves as a weak PM-targeting motif and that the motifs function additively. The two- to threefold enhancement of VLP production by PH- and myr/pal^{lyn}-gag-GFP was verified by western blot analysis examining the VLP fraction (data not shown). Overall, the GFP fluorescence-based VLP production assays were consistent with the microscopy observations indicating that the constructs that were able to target Gag to the PM were competent in VLP production (Figure 1c). These data indicate that the Gag constructs carrying *lyn* myr/pal or myr signals support VLP production more efficiently than the WT. Thus, we examined the infectivity of the lentiviral vectors produced by Gag with heterologous myr signals.

We constructed *gag-pol* derivatives bearing the myr/pal^{lyn} or myr^{lyn} sequences, and additional myr signal constructs carrying the myr signal of HIV-1 or MLV MA (myr^{HIV-1}- or myr^{MLV}-*gag-pol*, Figure 1a). These constructs were generated to examine whether any heterologous myr signal can function to enhance VLP production similar to the effect of the *lyn* acylation signal. In myr^{HIV-1}- or myr^{MLV}-*gag-pol*, the position of the myristoyl group is –22 amino acids upstream from the original Gag context, which is similar to the same position as myr/pal^{lyn} and myr^{lyn} mutants (Figure 1a). The expression of the *gag-pol* derivatives was verified by western blot analysis in which Pr55^{Gag} and its cleaved products by viral protease including MA-CA and p24^{CA} were detected (Figure 2a). These mutants produced VLP in the culture supernatant as verified by western blot analysis (Figure 2b). Using these *gag-pol* expression plasmids, in combination with the luciferase-encoding gene transfer plasmid and expression plasmids for Rev and VSV-G, we produced a lentiviral vector in 293FT cells. The viral production efficiencies were assessed by measuring the amount of viral capsid antigen p24^{CA}

a

Gag	MGARASVL...
G2A	MAARASVL...
PH-gag	(PLC delta 1 aa 1-175)-PRAE FTLAARASVL...
$CD4^{FL}$-gag	(CD4 aa 1-458)-E FTLAARASVL...
$CD4^{DC}$-gag	(CD4 aa 1-424)-E FTLAARASVL...
$CXCR4^{FL}$-gag	(CXCR4 aa 1-352)-EISSSSFE FTLAARASVL...
$CXCR4^{DC}$-gag	(CXCR4 aa 1-308)-ISSSSFE FTLAARASVL...
CD8-gag	(CD8 aa 1-235)-IDLELKL RILQSSSSFE FTLAARASVL...
Env-gag	(Env aa 1-869)-D PATGLRSRAE FTLAARASVL...
myr/pal^{lyn}-gag	MGCIKSKRKD NLNDDERRAE FTLAARASVL...
myr^{lyn}-gag	MGAIKSKRKD NLNDDERRAE FTLAARASVL...
pal^{lyn}-gag	MACIKSKRKD NLNDDERRAE FTLAARASVL...
Galpha(12)-gag	MS GVVRTLSRCL LPAEAGRRAE FTLAARASVL...
Galpha(13)-gag	MAD FLPSRSVCFP GCVLTNRRAE FTLAARASVL...
Galpha(16)-gag	MARSL RWRCCPWCLT EDEKAARRAE FTLAARASVL...
myr^{HIV-1}-gag	MGARASVLSG GELDRWRRAE FTLAARASVL...
myr^{MLV}-gag	MGQTVTTPLS LTLGHWRRAE FTLAARASVL...

b

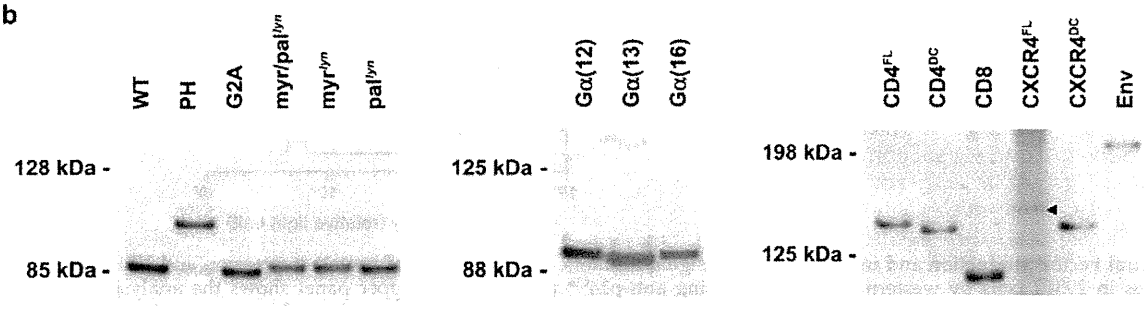

c

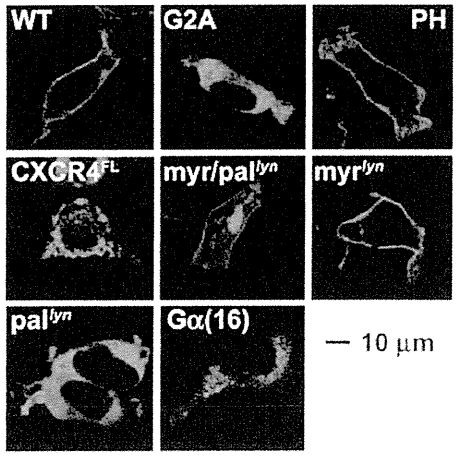

d VLP production efficiency (GFP fluorecence of VLP / cell fractions)

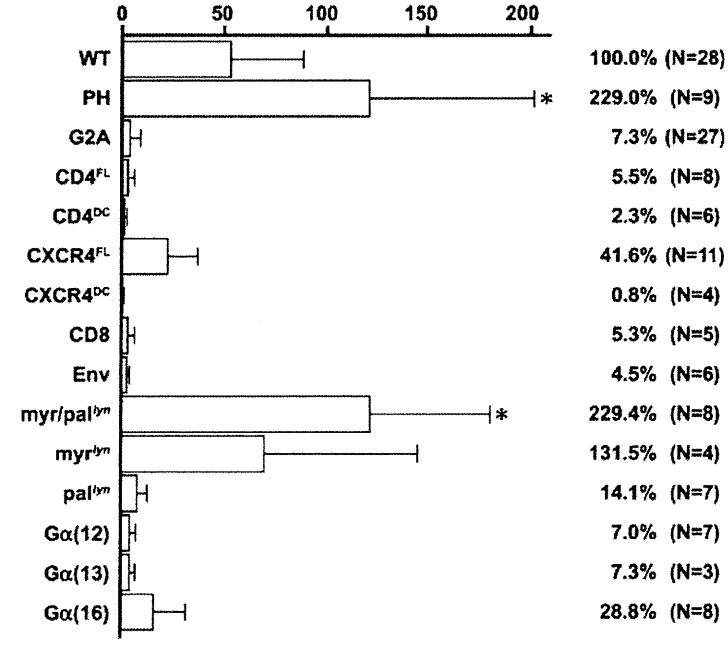

Figure 1 The production of VLPs by genetic modification of the PM-targeting signal of Gag. (**a**) The mutants used in this study. The myr site is marked with a dot, the palmitoylation site with an underline. The Gag translational initiation site and the myr target residues were mutated to leucine and alanine to minimize internal translational initiation and myr. (**b**) The verification of protein expression of Gag-GFP derivatives in 293FT cells by western blot analysis using anti-FLAG antibody. All the constructs carry the FLAG epitope at the C-terminus of Gag. The $CXCR4^{FL}$-Gag-GFP showed a low efficiency of detection, thus the immunoprecipitation was performed before immunoblotting (triangle). (**c**) The distribution of Gag-GFP derivatives in 293FT cells examined by confocal microscopy. WT represents the Gag-GFP, and the membrane-targeting signals are shown at the top of each panel. The bar represents 10 μm, magnification ×630. (**d**) VLP production efficiency of Gag-GFP derivatives measured by the GFP fluorescence in the VLP fraction divided by that of the cell fraction. The average and s.d. of the indicated number of independent experiments are shown. The VLP production efficiency relative to Gag-GFP is shown as a percentage at the right. Asterisks indicate the statistical significance compared with WT by two-tailed Student's *t*-test ($P<0.05$).

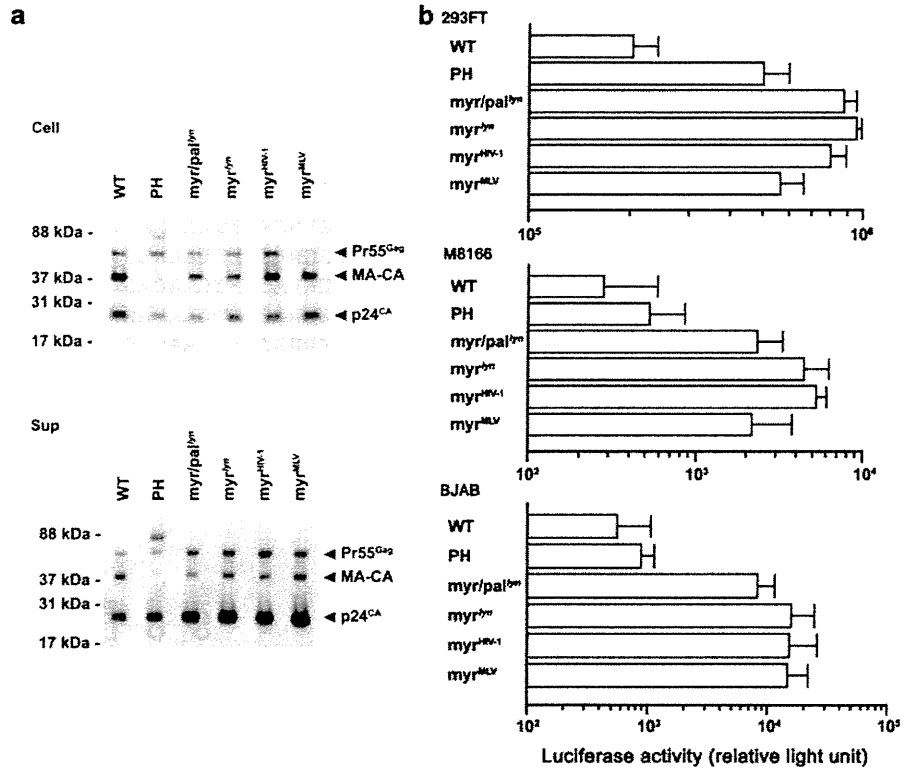

Figure 2 Lentiviral vector production and infectivity of myr signal mutants. (**a**) Verification of protein expression and VLP production of *gag-pol* derivatives in 293FT cells by western blot analysis using anti-p24^{CA} antibody. The upper panel shows the analysis of cell lysate equivalent to $1\sim2\times10^5$ cells (Cell). The lower panel shows the viral particles collected from the culture supernatant (Sup). Pr55^{Gag} (~55 kDa), the proteolytic cleavage intermediate of Pr55^{Gag} (MA-CA, ~40 kDa) and the complete proteolytic cleavage product p24^{CA} (~24 kDa) are indicated by arrowheads. PH-Gag has a higher molecular weight precursor and intermediate because of the PH domain of 23 kDa attached to the MA domain. (**b**) The transduction efficiency of the luciferase gene into various cell types. The 293FT, M8166 and BJAB cells were tested for luciferase gene transduction by the myr signal derivative lentivirus vectors. The *x* axis represents relative light emission. The average ± s.d. of luciferase activity assay in quadricate (293FT) or in triplicate (M8166 and BJAB) was shown. A representative data from three independent experiments is shown.

in the culture supernatant by enzyme-linked immunosorbent assay (ELISA). Enhancement of virus production by the PH, myr/pal^{lyn} and myr^{lyn} constructs was observed (4.1-, 6.3- and 10.5-fold increase in production, respectively, relative to the WT, Table 1). These data are consistent with the western blot analysis in which the levels of p24^{CA} are decreased from the cell fraction and increased in the VLP fraction for PH and myr signal mutants (Figure 2a). The magnitude of viral production enhancement was augmented in the *gag-pol* context compared with the Gag-GFP context. This is explained by the efficiency of Gag cleavage in the virion as described below. Viral production by the myr^{HIV-1}- or myr^{MLV}-*gag-pol* constructs also increased (6.2- or 6.1-fold, respectively, Table 1), suggesting that any heterologous myr signal can increase the production of lentiviral vector.

Luciferase gene transduction by lentiviral vectors produced using the modified Gag-pol was assessed in 293FT cells. The gene transduction efficiencies of *gag-pol* constructs were 6.1- to 10.9-fold greater than the WT (Figure 2b and Table 1). The luciferase activity decreased on treatment of the cells with the reverse transcriptase inhibitor nevirapine, suggesting that the luciferase activity indeed represents lentiviral gene transduction (data not shown). The increase in viral production by the heterologous myr signal constructs (4.3- to 7.8-fold compared with WT) largely agrees with the level of augmentation of luciferase activity (5.7- to 10.4-fold, Table 1). The myr/pal^{lyn} mutant showed a higher ratio (1.7) of luciferase transduction efficiency relative to viral production than the other myr signal mutants,

Table 1 Summary of viral production and infectivity of myr signal Gag mutants

	Viral production[a]	*Luciferase transduction*[b]	*Ratio*[c]
WT	1.0 ± 0.0 (n = 17)	1.0 ± 0.0 (n = 15)	1.0
PH	4.1 ± 0.9 (n = 17)**	6.3 ± 1.8 (n = 15)*	1.5
myr/pal^{lyn}	6.3 ± 1.8 (n = 17)*	10.4 ± 2.7 (n = 15)**	1.7
myr^{lyn}	10.5 ± 3.4 (n = 13)*	9.2 ± 3.2 (n = 11)*	0.9
myr^{HIV-1}	6.2 ± 1.9 (n = 12)*	5.7 ± 1.5 (n = 10)*	0.9
myr^{MLV}	6.1 ± 1.1 (n = 12)**	7.6 ± 2.7 (n = 10)*	1.2

Abbreviations: HIV-1, human immunodeficiency virus type 1; MLV, murine leukemia virus; myr, myristoylation; pal, palmitoylation; PH, pleckstrin homology; WT, wild type.
[a]The average ± s.e.m. of the p24^{CA} concentration relative to WT from the indicated number of independent experiments.
[b]The average ± s.e.m. of transduced luciferase activity relative to WT from the indicated number of independent experiments.
[c]The luciferase transduction divided by viral production.
Asterisks indicate a statistically significant difference compared to the WT by two-tailed Student's paired *t*-test (*P < 0.05, **P < 0.01).

suggesting that the infectivity of the myr/pal^{lyn} virus particles is slightly improved (Table 1). Luciferase gene transduction by myr signal constructs was also observed in the B lymphoid cell line BJAB and T lymphoid cell line M8166, similar to 293FT cells (Figure 2b). Gene transduction of GFP by myr signal *gag-pol* constructs was comparable to transduction of the luciferase gene (data not shown). Collectively, these results indicate that extending the amino-terminus of Gag with a heterologous myr signal enhances infectious lentiviral production.

We analyzed the molecular mechanisms by which viral production was improved by the amino-terminal Gag modifications. We examined (i) the oligomerization efficiency, (ii) the Vps4-dependence of viral budding, (iii) Gag targeting to the Triton X-100-insoluble lipid (detergent-resistant membrane, DRM) fraction and (iv) the morphology of the virion. First, the oligomerization efficiency was measured using a bioluminescent resonance energy transfer (BRET) assay (Figure 3a). The 293FT cells were co-transfected with plasmids expressing Gag derivatives fused to GFP or renilla luciferase (Rluc), and the GFP fluorescence activated by the Rluc-emitted light was measured in living cells. This BRET signal should represent the self-oligomerization efficiency of Gag derivatives *in vivo*. The GFP–Rluc fusion protein should yield the best BRET efficiency, and was thus used as the positive control. Rluc alone should not yield any BRET signal, and thus was used as a negative control. We focused on the derivatives that showed enhanced viral production. The BRET levels of all the tested mutants were significantly increased compared with the WT Gag (Figure 3a). These data imply that the assembly of the myr signal Gag constructs is more efficient than the WT. It is conceivable that the enhanced VLP production of myr signal Gag constructs is, in part, because of improved assembly efficiency. Efficient Gag assembly should also assist the Gag-pol assembly. The Gag-pol assembly leads to the activation of a viral protease that cleaves Gag to make the virus infectious. Provided that the myr signal Gag mutants can efficiently activate the viral protease, we expected that the Gag processing of myr signal Gag constructs should be more efficient than the WT. Virions were collected by centrifugation and processed for western blotting using the anti-p24^{CA} monoclonal antibody (mAb). Anti-p24^{CA} mAb binds to Pr55^{Gag} and its cleaved products including MA-CA and p24^{CA}. The p24^{CA} signal relative to the Pr55^{Gag} and MA-CA represents the Gag processing efficacy. Compared with cell lysates (Figure 2a), viral lysates showed better Gag cleavage for all samples (Figure 3b). The WT virions showed a substantial amount of Gag intermediates (Figure 3b). In contrast, only trace amounts of intermediate were detected in the myr signal construct virions (Figure 3b). It is possible that the enhanced Gag processing is due to the increased Gag-pol to Gag ratio in the virion produced by myr Gag mutants. We tested this possibility by western blot analysis probing p24^{CA} and integrase (IN) at the same time. IN represents the Gag-pol because IN is one of the proteolytic products generated from Gag-pol. The signal intensities of IN (open arrowhead, Figure 3b) relative to p24^{CA} (filled arrowhead, Figure 3b) for myr signal mutants were comparable to WT, suggesting that enhanced Gag processing is not due to the increased Gag-pol to Gag ratio in the virion

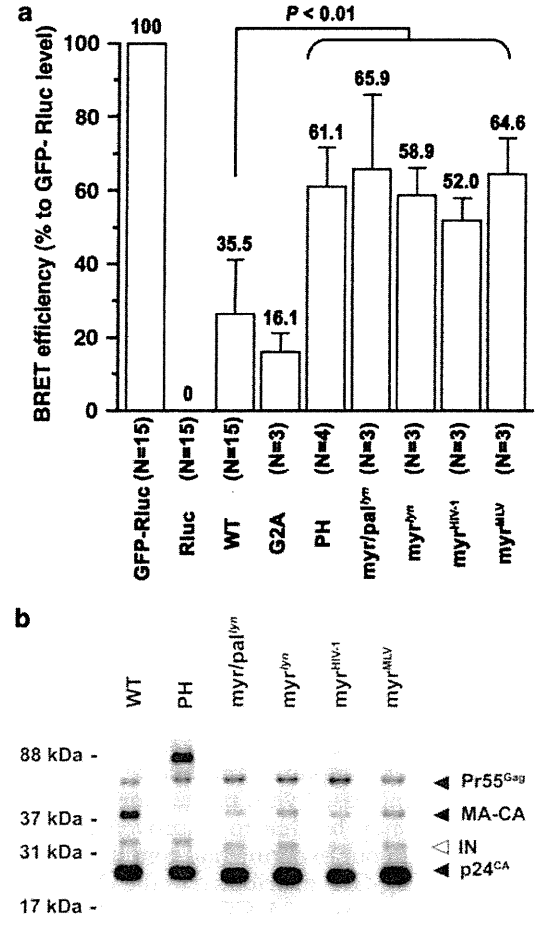

Figure 3 The physical and functional properties of myr signal derivatives of Gag. (**a**) Gag oligomerization examined by BRET analysis. The GFP–Rluc fusion protein and Rluc alone were used as positive and negative controls. The average ± s.d. of BRET efficiencies relative to the controls obtained in the indicated number of experiments are shown. All the *gag* mutants yielded significantly higher BRET signals than that of WT as analyzed by two-tailed Student's *t*-test ($P<0.01$). (**b**) The Gag processing and the Gag to Gag-pol ratio in the virion was tested by western blot analysis using anti-p24^{CA} and anti-IN monoclonal antibodies. Note that the samples were loaded to yield similar p24^{CA} signals to highlight the differences in Gag cleavage efficiencies and Gag to Gag-pol ratio. The virion was collected from the culture supernatant of cells shown in Figure 2a. Pr55^{Gag}, MA-CA, p24^{CA} (filled) and IN (open) are indicated by arrowheads.

produced by myr Gag constructs. Collectively, the results suggest that the heterologous myr signals enable Gag to assemble with a higher efficiency, leading to the activation of protease to process Gag more efficiently in the virion. This should account for the fact that the magnitude of difference between WT and mutants in VLP production was assessed greater by p24 ELISA assay using *gag-pol* constructs than by GFP fluorescence-based assay using Gag-GFP constructs.

Second, the Vps4-dependence of VLP budding was examined. Vps4 drives HIV-1 budding.[15] We measured VLP production efficiencies by *gag-pol* derivatives in the presence or absence of a dominant-negative Vps4. If VLP budding is powered by a Vsp4-independent mechanism, expression of dominant-negative Vps4 should not reduce the VLP production efficiency. Viral gene expression was

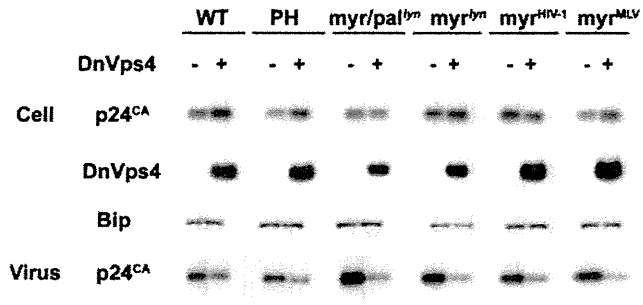

Figure 4 The effect of dominant-negative Vps4 (DnVps4) on virus production by acylation signal Gag derivatives. DnVps4 expression did not lower Gag expression in transiently transfected 293FT cells. In contrast, the virus production by all the Gag constructs was inhibited by DnVps4, similar to the WT.

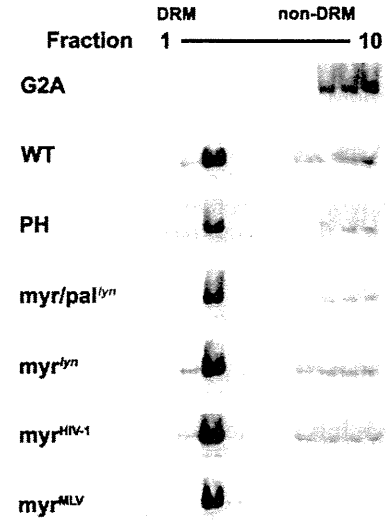

Figure 5 The targeting of Gag-GFP derivatives to the DRM fraction examined by a membrane floatation assay. G2A construct distributed to the non-DRM fractions (lanes 8–10), and WT Gag was targeted to the DRM (lanes 2–3). Other mutants distributed to the DRM fractions similar to WT Gag. All the derivatives were probed with anti-FLAG antibody.

not inhibited by dominant-negative Vps4 expression as judged by p24^{CA} levels (Figure 4). However, on expression of dominant-negative Vps4, viral production decreased in all the mutants (the lower panel of Figure 4), suggesting that the amino-terminal modification of Gag does not alter the molecular mechanism of viral budding.

Third, DRM targeting was examined using membrane floatation assays. Gag has previously been shown to form higher order complexes and bud at DRM-containing regions.[16,17] Increased viral production by myr signal Gag constructs may be due to improved efficiency of DRM targeting. In our experimental conditions, approximately 70% of Gag-GFP distributed to the DRM fractions (Figure 5). In contrast, G2A-GFP distributed predominantly to the non-DRM fractions (Figure 5). These data are consistent with the microscopy observations and previous reports (Figure 1c and Lindwasser and Resh[16] and Ono and Freed[17,18]). The myr signal derivatives accumulated in the DRM fractions at levels similar to the WT (Figure 5). These data suggest that enhanced viral production is not due to enhanced DRM targeting of Gag with amino-terminal modifications.

Finally, the morphology of the virion was analyzed using TEM. We compared the morphology of the WT and the myr^{lyn}-*gag-pol* virions. The morphology of budding and mature virions of myr^{lyn}-*gag-pol* construct was indistinguishable from the WT (Figure 6).[14] In addition, VSV-G was incorporated into the virion produced by myr signal derivatives at levels similar to the WT (data not shown). Similar observation was made for the incorporation of HIV-1 Env onto the virion (data not shown). The myr^{HIV-1}- and myr^{MLV}-Gag-GFP showed a PM-targeting phenotype similar to the WT as judged by confocal microscopy (data not shown). Taken together, lentiviral vectors bearing amino-terminally engineered Gag can produce virions with greater efficiencies than the original lentiviral vector. This increase was primarily attributed to the effects of the increased efficiency Gag oligomerization.

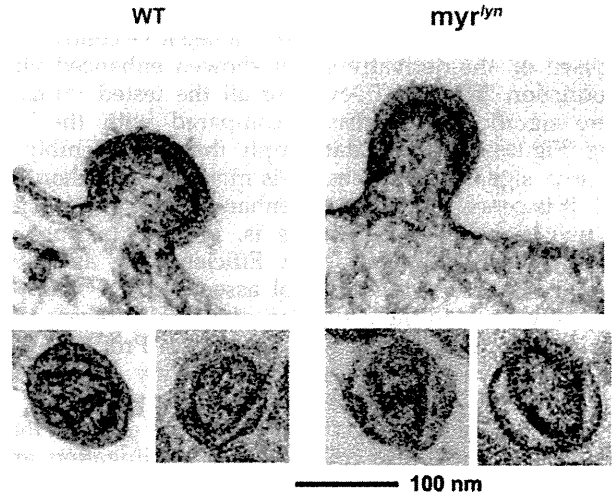

Figure 6 The morphology of virions produced from 293FT cells transiently transfected with *gag-pol* (WT, left) or myr^{lyn}-*gag-pol* (right) expression vector. The upper panels show viral budding at the cell periphery, and the lower panels show the morphology of virions found in the extracellular space. The bar represents 100 nm, magnification × 50 000.

Discussion

In this study, we have provided evidence that genetic modification of the structural protein Gag can improve the virion production efficiency of the HIV-1-based lentiviral vector up to 10-fold. Our technology will provide an improved lentiviral vector for human gene therapy applications, which require large-scale viral vector preparation. Historically, efforts to improve the lentiviral vector have not involved the modification of the structural protein Gag.[9] Our strategy is unique in this regard. Our viral vector can be defined as a next generation lentiviral vector. This approach may also be worth testing for murine leukemia virus (MLV)-based vectors because the function of the MLV Gag is dependent on amino-terminal myr sites, similar to HIV Gag.

Our genetic approach revealed that amino-terminal modifications that re-position the myristoyl group attachment site on Gag can alter the late phases of the HIV-1 life cycle. Gag traffics to the PM efficiently, and the myristoyl group is critical for this process.[19] The myristoyl group attached to Gag is in equilibrium between exposed and folded 'hidden' conformations.[20] The PM targeting of Gag depends primarily on myristoyl group exposure. It is possible that re-positioning of the myristoyl group on Gag may slightly shift the structural equilibrium toward the exposed conformation, which facilitates PM targeting by Gag. However, myr signal Gag mutants did not show higher DRM-targeting efficiencies than WT (Figure 5). We performed the membrane floatation assay without Triton X-100 and found that the myr signal Gag mutants and WT distributed to the membrane fraction at similar efficiencies (data not shown). These data may suggest that the myristoyl group exposure model is unlikely. However, these data may not necessarily negate the myristoyl group exposure model because it is possible that the steady-state levels of Gag association with DRM could be saturable. Alternative hypothesis is that the re-positioning of myristoyl group may stabilize the Gag-PM association or Gag–Gag interaction, both of which should lead to an increased viral production.

Membrane proteins do not serve as an ideal PM-targeting motif for improvement of the lentiviral vector. The substitution of myr signal with membrane proteins appears to be less favorable because the PM-targeting efficiency of the membrane protein constructs was not high enough to produce VLP, probably because Gag starts to assemble on the ER membrane and bud into intracellular membrane compartments. This premature assembly may block the efficient ER exit of the membrane protein-Gag derivatives. In 293FT cells transiently transfected with plasmids expressing membrane Gag mutants, high electron density signals on the intracellular membranes and PM, representing assembled membrane protein-Gag mutants, were observed (data not shown). In addition, intracellular VLP formation was observed in intracellular membrane compartments surrounding the nucleus (data not shown). These observations were consistent with the confocal microscopy data, and suggest that the membrane protein-Gag constructs are assembly-competent. Interestingly, the morphology of the intracellular virion of CXCR4^{DC}-*gag-pol* was similar to late domain-defective HIV-1 particles. These data may imply that the membrane protein-Gag derivatives are not fully competent in VLP formation and/or release.

Considering our data, HIV-1 could have evolved to be able to produce more virus particles than it does now. However, such a virus was not selected in nature. This is presumably because the increased viral production may not confer a strong selective advantage for HIV-1 to spread in human population. It is possible that such a virus may kill the host, resulting in the loss of opportunity to be transmitted to a new host. Alternatively, such a virus may be more immunogenic, thus have selective disadvantage in the host. Conversely, it is possible that HIV-1 has already evolved to bud from its natural target cells, namely CD4-positive T lymphocytes or macrophages. If this is the case, our experimental observation might be only applied to the lentiviral vector production in 293FT cells.

Our next generation lentiviral vector should contribute to an increase in lentiviral vector applications, as a tool both for molecular biology research and for human gene therapy. The safety concerns involving Gag amino-terminal modification should be critically examined to use the modified lentiviral vector in clinical trials because the effect of amino-terminal modification of Gag on the lentiviral life cycle is unpredictable. The amino-terminal modification of Gag may alter the chromosomal integration site preference of the lentiviral vector genome. A genome-wide survey to determine the cellular genomic loci in which the Gag-modified lentiviral vector preferentially inserts its genome, compared with the original viral vector, should be conducted. In addition, it may be important to measure the frequency of insertional oncogenesis using small animal models. It is also possible that the fidelity of reverse transcription could be affected by the Gag amino-terminal modification. If the accuracy of reverse transcription drops, the therapeutic effect of the modified lentiviral vector might be affected. These issues should be addressed before the modified lentiviral vector is applied to human gene therapy.

We may be able to further improve the lentiviral vector using systematic modifications of Gag, but such an approach has yet to be examined. For example, the positioning the myr attachment site in all the myr signal Gag derivatives tested in this study was –22 amino acids relative to the original position. A better myristol group-positioning site or other PM-targeting signals to boost viral production and infectivity could be identified by performing an exhaustive systematic modification study.

Materials and methods

Plasmids

The codon optimized HIV-1 *gag* was amplified by PCR from pSyn HIV-1 *gag-pol*[21] using the following primers: HIV-1 *gag* forward 5′-ACCGGTCTCGAGCCACCAT GGGCGCCAGGGCCAGCGTGCTGAGC-3′, HIV-1 *gag* reverse 5′-TCATTGGATCCGGTCGTCATCGTCTTTGT AGTCTTGTGACGAGGGGTCGTTGCCAAAG-3′. The PCR fragment was cloned into pCR4 Blunt TOPO (Invitrogen, Tokyo, Japan), digested with *Xho*I–*Bam*HI, and the resulting fragment was cloned into the *Xho*I–*Bam*HI sites of pEGFP-N2 (Clontech, Palo Alto, CA, USA), generating pGag-GFP. A FLAG epitope tag was encoded at the carboxy-terminus of Gag. The LA-*gag* has been described previously.[14] The *Sna*BI–*Sac*II fragment from pLA-*gag-pol* was cloned into the *Sna*BI–*Sac*I sites of pSyn HIV-1 *gag-pol*, generating the pLA-*gag*-GFP.

The CD4 FL or DC was amplified from CD4 complementary DNA[22] using the following primers: FL and DC forward 5′-GGATCCCGGGCCACCATGAACCG GGGAGTCCCTTTTAGGC-3′, FL reverse 5′-GAATT CAATGGGGCTACATGTCTTCTGAAACCGG-3′, and DC reverse 5′-GAATTCGTGCCGGCACCTGACACAGAAG AAGATGCC-3′. The PCR fragments were cloned into pCR4 Blunt TOPO (Invitrogen), digested with *Bam*HI–*Eco*RI, and the resulting fragments were cloned into the *Bgl*II*Eco*RI sites of pEGFP-N2, generating pCD4$^{FL/DC}$-GFP. The *Sna*BI–*Eco*RI fragments from pCD4$^{FL/DC}$-GFP were cloned into the corresponding sites of pLA-*gag*-GFP, generating pCD4$^{FL/DC}$-*gag*-GFP.

The full-length human CD8 ORF was amplified by reverse transcriptase-PCR using mRNA isolated from peripheral blood mononuclear cell (PBMC) with following primers: 5′-GCTAGCATGGCCTTACCAGTGAC-3′and 5′-AGATCTATGACGTATCTCGCCGAAAGGCT-G-3′. An *Nhe*I–*Bgl*II fragment was cloned into the corresponding sites of pEGFP-N1 (Clontech), generating pEGFPN1hCD8. The *Sna*BI–*Sal*I fragment from pEGFPN1hCD8 was cloned into the *Sna*BI–*Xho*I site of pCXCR4^{FL}-*gag*-GFP, generating pCD8-*gag*-GFP.

The CXCR4 FL and DC were amplified from the CXCR4 complementary DNA[22] using the following primers: FL and DC forward 5′-ACCGGTGCCACCATG GAGGGGATCAGTATATACACTTCAG-3′, FL reverse 5′-AGATCTCGCTGGAGTGAAAACTTGAAGACTCAGA CTC-3′, and DC reverse 5′-AGATCTTGGCTCCAAG GAAAGCATAGAGGATGGG-3′. The *Age*I–*Bgl*II fragments of the PCR products were cloned into *Age*I–*Bgl*II sites of pEGFP-C2, generating pCXCR4$^{FL/DC}$-GFP. The *Sna*BI–*Eco*RI fragments from pCXCR4$^{FL/DC}$-GFP were cloned into the corresponding sites of pLA-*gag*-GFP, generating pCXCR4$^{FL/DC}$-*gag*-GFP.

The following oligonucleotides were annealed and cloned into the BsrGI site of pEGFP-N2 to generate pEGFP-N2-FLAG: 5′-GTACGACTACAAAGACGATGA CGACTATAAGTAAGC-3′ and 5′-GGCCGCTTACTTA TAGTCGTCATCGTCTTTGTAGTC-3′. HIV-1 Env was amplified from pgp160opt that encodes a codon-optimized gp160 (obtained through the NIH AIDS Research and Reference Reagent Program[23]) using the following primers: 5′-GGAACTGGTTCGACATCACCAAGTGGCT GTGG-3′ and 5′-GTTAACCCCGGGATCCAGCAGGGC GGTCTCGAAGCCCTGGCGGATGCGGC-3′. The *Bgl*II–*Xma*I fragment of the PCR product was cloned into pEGFP-N2 flag, generating pgp160opt3fwd2revEGFPN2f. The *Nde*I–*Sfi*I fragment from pgp160opt was cloned into pgp160opt3fwd2revEGFPN2f, generating pgp160optGFPf. The *Afe*I–*Mfe*I fragment carrying *gag*-GFP was cloned into the pgp160optGFPf, generating pEnv-*gag*-GFP.

The PH domain of phospholipase C-δ1 from pGFP-PH (generous gift from Dr Meyer's group,[24]) was amplified using following primers: forward 5′- CGCTAGCACC GGTGCCACCATGGACTCGGGCCGGGACTTCCTG-3′ and reverse 5′- CCTCGAGGCTGGATGTTGAGCTCCTT CAGG-3′. The *Nhe*I–*Xho*I fragment of the PCR product was cloned into the corresponding sites of pLA-*gag*-GFP, generating pPH-*gag*-GFP.

The following oligonucleotides were annealed and inserted into the *Nhe*I–*Xho*I sites of pLA-*gag*-GFP to generate pmyr/pal^{lyn}-*gag*-GFP, pmyr^{lyn}-*gag*-GFP, ppal^{lyn}-*gag*-GFP, pGα (12)-*gag*-GFP, pGα (13)-*gag*-GFP, pGα (16)-*gag*-GFP, pmyr^{MLV}-*gag*-GFP, pmyr^{HIV-1}-*gag*-GFP: myr/pal^{lyn} forward 5′- CTAGCGCCACCATGGGCTGCAT CAAGTCCAAGCGGAAGGACAACTTGAACGACGAC GAGCG-3′ and myr/pal^{lyn} reverse 5′- TCGACGCTC GTCGTCGTTCAAGTTGTCCTTCCGCTTGGACTTGAT GCAGCCCATGGTGGCG-3′; myr^{lyn} forward 5′- CTAGC GCCACCATGGGCGCCATCAAGTCCAAGCGGAAGG ACAACTTGAACGACGACGAGCG-3′ and myr^{lyn} reverse 5′- TCGACGCTCGTCGTCGTTCAAGTTGTCCT TCCGCTTGGACTTGATGGCGCCCATGGTGGCG-3′; pal^{lyn} forward 5′- CTAGCGCCACCATGGCATGTATTAA ATCAAAAAGGAAAGACCg-3′ and pal^{lyn} reverse 5′- TC GACGGTCTTTCCTTTTTGATTTAATACATGCCATGGT GGCG-3′; Gα(12) forward 5′- CTAGCGCCACCATGT CCGGCGTGGTGCGGACCCTGTCCCGGTGCCTGCTG CCCGCCGAAGCCGGCCG-3′ and Gα(12) reverse 5′- TC GACGGCCGGCTTCGGCGGGCAGCAGGCACCGGGA CAGGGTCCGCACCACGCCGGACATGGTGGCG-3′; Gα(13) forward 5′- CTAGCGCCACCATGGCCGACTTC CTGCCCTCCCGGTCCGTGTGCTTCCCCGGCTGCGTG CTGACCAACCG-3′ and Gα(13) reverse 5′- TCGACGG TTGGTCAGCACGCAGCCGGGGAAGCACACGGACCG GGAGGGCAGGAAGTCGGCCATGGTGGCG-3′; Gα(16) forward 5′- CTAGCGCCACCATGGCCCGGTCCCTGCG GTGGCGGTGCTGCCCCTGGTGCCTGACCGAGGACGA GAAGGCCGCCCG-3′ and Gα(16) reverse 5′- TCGAC GGGCGGCCTTCTCGTCCTCGGTCAGGCACCAGGGGC AGCACCGCCACCGCAGGGACCGGGCCATGGTGGC G-3′; myr^{HIV-1} forward 5′- CTAGCGCCACCATGGGCG CCAGGGCCAGCGTGCTGAGCGGCGGCGAGCTGGAC AGGTGGCG-3′ and myr^{HIV-1} reverse 5′- TCGACGC CACCTGTCCAGCTCGCCGCCGCTCAGCACGCTGGCC CTGGCGCCCATGGTGGCG-3′; myr^{MLV} forward 5′- CTA GCGCCACCATGGGCCAGACTGTTACCACTCCCTTAAG TTTGACCTTAGGTCACTGGCG-3′ and myr^{MLV} reverse 5′- TCGACGCCAGTGACCTAAGGTCAAACTTAAGGGA GTGGTAACAGTCTGGCCCATGGTGGCG-3′. The *Sna*a-BI–*Sac*II fragments from pmyr/pal^{lyn}-*gag*-GFP, pmyr^{lyn}-*gag*-GFP, pmyr^{MLV}-*gag*-GFP and pmyr^{HIV-1}-*gag*-GFP were cloned into the corresponding sites of pSyn HIV-1 *gag-pol* to generate pmyr/pal^{lyn}-*gag-pol*, pmyr^{lyn}-*gag-pol*, pmyr^{MLV}-*gag-pol* and pmyr^{HIV-1}-*gag-pol*, respectively.

The following linkers were inserted into the *Bam*HI site of the pGag-GFP, to generate the pHIV-1 *gag*f AB linker: 5′-GATCAAGGATCCACCGGTAGATCTGACCG GTGGATCCTT-3′ and 5′-GATCAAGGATCCACCGGT CAGATCTACCGGTGGATCCTT-3′. The firefly luciferase open reading frame was amplified by PCR using the following primers: 5′-ACCGGTCTCGAGGGCCAC CATGGAAGACGCCAAAAACATAAAGAAAGG-3′ and 5′-GAATTCGGATCCTTACACGGCGATCTTTCCGCCCT TCTTGGCC-3′. The *Age*I–*Eco*RI fragment of the PCR product was cloned into the *Bam*HI site of the pHIV-1 *gag*f AB linker, producing pGag-fLuc. The *Nhe*I–*Xba*I fragment from phRL-CMV (Promega, Tokyo, Japan) was inserted into the *Bam*HI site of pGag-fLuc, generating the pGag-Rluc II, using the following linkers: *Nhe*I side, 5′-GATCTGGTTACCCAATTG-3′ and 5′-CTAGCAATTG GGTAACCA-3′; *Xba*I side, 5′-CTAGCGAATTCA-3′ and 5′-GATCTGAATTCG-3′.

The *Nde*I–*Sac*II fragment from pPH-*gag*-GFP[14] was cloned into the corresponding sites of pGag-Rluc II, generating pPH-*gag*-Rluc. The *Apa*I–*Hpa*I fragments from pmyr/pal^{lyn}-*gag*-GFP, pmyr^{lyn}-*gag*-GFP, pmyr^{MLV}-*gag*-GFP and pmyr^{HIV-1}-*gag*-GFP were cloned into the corresponding sites of pGag-Rluc II, generating pmyr/pal^{lyn}-*gag*-Rluc, pmyr^{lyn}-*gag*-Rluc, pmyr^{MLV}-*gag*-Rluc and pmyr^{HIV-1}-*gag*-Rluc, respectively.

The Vps4DN expression vector was the generous gift of Dr H Gottlinger (University of Massachusetts). Other plasmids including pLenti-luciferase, pVSV-G and pRevpac have been described previously.[14]

Cells and transfection

Cells were maintained in RPMI 1640 medium (Sigma, St Louis, MA, USA) supplemented with 10% fetal bovine serum (Japan Bioserum, Tokyo, Japan), 50 U ml^{-1} penicillin and 50 μg ml^{-1} streptomycin (Invitrogen), at 37 °C in a humidified 5% CO_2 atmosphere. Cells were

transfected with Lipofectamine 2000 according to the manufacturer's protocol (Invitrogen).

Western blotting

Transfected 293FT cells were washed once with Dullbeco's phosphate-buffered saline (Sigma), centrifuged and lysed in a buffer containing 0.31 M Tris-HCl (pH 6.8), 10% (w/v) sodium dodecyl sulfate, 50% (v/v) glycerol, 500 mM dithiothreitol and 0.25% (w/v) bromophenol blue. Proteins were separated by sodium dodecyl sulfate–polyacrylamide gel electrophoresis and transferred to polyvinylidine difluoride membranes (Millipore, Tokyo, Japan). Membranes were incubated with primary antibodies including polyclonal anti-flag (Rockland Immunochemicals, Gilbertsville, PA, USA), anti-$p24^{CA}$ mAb clone 183-H12-5C (NIH AIDS Research and Reference Reagent Program), anti-HIV-1 IN mAb clone ab72007 (Abcam, Cambridge, MA, USA) or anti-Bip mAb clone 40 (BD Biosciences, Tokyo, Japan), followed by a horseradish peroxidase conjugated secondary antibody (Envision, Dako, Tokyo, Japan). Chemiluminescence was generated using Lumilight (Roche, Tokyo, Japan) or Lumigen (GE Healthcare, Tokyo, Japan). Signals were detected using an LAS-3000 mini Lumino-Image analyzer operated by the LAS-300 mini Image Reader software (ver.2.2, Fuji Film, Tokyo, Japan). The brightness and contrast of the image were adjusted using Adobe Photoshop (ver.7.0, Adobe, Tokyo, Japan).

Confocal microscopy

Transfected 293FT cells were grown on slide glass in the presence of Hoechst 33258 (Sigma) for 24 h, fixed (4% formaldehyde), mounted and analyzed using confocal fluorescence microscopy (LSM510 Meta 63 × NA 1.4 lens, Carl Zeiss MicroImaging Inc., Tokyo, Japan). The brightness and contrast of the image were adjusted using the LSM image browser (Carl Zeiss).

VLP assay

Transfected 293FT cells were washed once with phosphate-buffered saline, centrifuged and lysed in buffer A (150 mM NaCl, 50 mM Tris-HCL (pH 8.0), 0.5% IGEPAL CA-630) for 0.5–1 h on ice (cell fraction). The cell culture medium was collected, passed through a 0.45 μm filter, and VLP were pelleted by ultracentrifugation (541 k × *g* for 1 h). The VLP pellet was lysed in buffer A for 0.5–1 h (VLP fraction). The green fluorescent intensities of cell and VLP fractions were quantified with a DTX880 Multimode Detector (excitation 485 nm, emission 535 nm) (Beckman Coulter, Tokyo, Japan). The efficiency of VLP production was calculated by dividing the green fluorescent intensity of the VLP fraction by that of the cell fraction.

Infection with lentiviral vector

The 293FT cells grown in six-well plates were transfected with *gag-pol* vector (1 μg), pLenti-luciferase (0.65 μg), pVSV-G (0.4-0.8 μg) or pRevpac (0.05 μg) using Lipoftamine 2000, and replated into three wells of a six-well plate at 4–6 h after transfection. At 48 h after transfection, the cell culture medium was collected, passed through a 0.45 μm filter (Millex-HV polyvinylidine difluoride; Millipore), and mixed with dextran (final concentration 16.25 μg ml^{-1}; DEAE-Dextran chloride, MW ~500 kDa; ICN Biomedicals Inc., Aurora, OH, USA). The 293FT cells at 50% confluency in 24-well plates were exposed to 800 μl of cell culture medium containing viruses. At 4–6 h after infection, 293FT cells were split into 4 wells of a 48-well plate. At 48 h after infection, the luciferase activity was measured using the Steady-Glo Luciferase Assay system (Promega). Luminescence was detected using a Veritas Microplate Luminometer (Promega).

Enzyme-linked immunosorbent assay

A p24 ELISA was conducted according to the manufacturer's protocol (Zeptometrics, Buffalo, NY, USA). To measure cellular p24, transfected 293FT cells were washed once with phosphate-buffered saline, lysed in 500 μl buffer A (described above) for 30 min, and subjected
to the ELISA.

Bioluminescence resonance energy transfer

The basic protocol for the BRET assay has been described previously.[25] Briefly, 293FT cells grown in a six-well plate were transfected with 0.05–0.2 μg of expression plasmids for Gag derivatives fused to the Rluc together with 1–2 μg of Gag derivatives fused to GFP. At 48 h after transfection, cells were collected and incubated with the Rluc substrate according to the manufacturer's protocol, with the exception that a 5- to 10-fold higher substrate concentration was used (ViviRen Live Cell Substrate; Promega). We measured BRET signals under the conditions in which the GFP and Rluc expression levels were almost similar among the tested samples. The fluorescent and bioluminescent signals were measured using a Tristar LB941 instrument (Berthold Technologies, Bad Wildbad, Germany).

Membrane floatation assay

293FT cells were transfected with a *gag* expression vector using Lipofectamine 2000 (Invitrogen) according to the manufacturer's protocol. At 48 h after transfection, cells were rinsed with ice-cold phosphate-buffered saline and centrifuged at 600 × *g* for 5 min. Cell pellets were resuspended in a buffer containing 10 mM Tris-Cl (pH 7.5), 4 mM EDTA and protease inhibitor cocktail (Sigma), and sonicated on ice. Cell lysates were centrifuged at 370 × *g* for 3 min. A 120 μl aliquot of supernatant was mixed with 3.6 μl 5 M NaCl (final concentration = 150 mM) and 120 μl of TNE-T (100 mM Tris-Cl (pH 7.5), 600 mM NaCl, 16 mM EDTA and 0.5% Triton X-100). These samples were placed on ice for 20 min. Subsequently, 200 μl of supernatant was mixed with 1 ml of 85.5% (wt/vol) sucrose in TNE and placed on the bottom of a centrifuge tube (Ultra Clear, Beckman Coulter), overlayed with 2.8 ml 65% and 1.2 ml 10% (wt/vol) sucrose in TNE-T without Triton X-100 (TNE), respectively. The gradient solution was centrifuged for 16 h at 1 48 862 × *g* at 4 °C in a BECKMAN SW55Ti rotor and 10 fractions of 500 μl each were recovered from top-to-bottom.

Transmission electron microscopy (TEM)

Transmission electron microscopy imaging was conducted by Hanaichi Co Ltd (Okazaki, Japan). Transfected 293FT cells were removed culture medium, fixed (2% glutaraldehyde, 2% osmium tetroxide), and imaged by transmission electron microscopy (at 100 kV;

JEOL JEM2000EX, Japan Electron Optics Laboratory Co., Ltd., Tokyo, Japan).

Conflict of interest

The authors declare no conflict of interest.

Acknowledgements

This work was supported by the Japan Health Science Foundation, the Japanese Ministry of Health, Labor and Welfare (H18-AIDS-W-003 to JK) and the Japanese Ministry of Education, Culture, Sports, Science and Technology (18689014 and 18659136 to JK).

References

1 MacGregor RR. Clinical protocol. A phase 1 open-label clinical trial of the safety and tolerability of single escalating doses of autologous CD4T cells transduced with VRX496 in HIV-positive subjects. *Hum Gene Ther* 2001; **12**: 2028–2029.
2 Hofling AA, Devine S, Vogler C, Sands MS. Human CD34+ hematopoietic progenitor cell-directed lentiviral-mediated gene therapy in a xenotransplantation model of lysosomal storage disease. *Mol Ther* 2004; **9**: 856–865.
3 Bank A, Dorazio R, Leboulch P. A phase I/II clinical trial of beta-globin gene therapy for beta-thalassemia. *Ann NY Acad Sci* 2005; **1054**: 308–316.
4 Manilla P, Rebello T, Afable C, Lu X, Slepushkin V, Humeau LM *et al.* Regulatory considerations for novel gene therapy products: a review of the process leading to the first clinical lentiviral vector. *Hum Gene Ther* 2005; **16**: 17–25.
5 Cockrell AS, Kafri T. Gene delivery by lentivirus vectors. *Mol Biotechnol* 2007; **36**: 184–204.
6 Lundberg C, Björklund T, Carlsson T, Jakobsson J, Hantraye P, Déglon N *et al.* Applications of lentiviral vectors for biology and gene therapy of neurological disorders. *Curr Gene Ther* 2008; **8**: 461–473.
7 Maetzig T, Galla M, Brugman MH, Loew R, Baum C, Schambach A. Mechanisms controlling titer and expression of bidirectional lentiviral and gammaretroviral vectors. *Gene Ther* 2010; **17**: 400 .
8 ter Brake O, Berkhout B. Lentiviral vectors that carry anti-HIV shRNAs: problems and solutions. *J Gene Med* 2007; **9**: 743–750.
9 McCart JA, Bartlett DI. Lentiviral vectors. In: Templeton NS (ed). *Gene and Cell Therapy: Therapeutic Mechanisms and Strategies*, rd edn CRC Press: Carrollton, 2008, pp 245–262.
10 Fiorentini S, Marini E, Caracciolo S, Caruso A. Functions of the HIV-1 matrix protein p17. *New Microbiol* 2006; **29**: 1–10.
11 Hearps AC, Jans DA. Regulating the functions of the HIV-1 matrix protein. *AIDS Res Hum Retroviruses* 2007; **23**: 341–346.
12 Bukrinskaya A. HIV-1 matrix protein: a mysterious regulator of the viral life cycle. *Virus Res* 2007; **124**: 1 .
13 Klein KC, Reed JC, Lingappa JR. Intracellular destinies: degradation, targeting, assembly, and endocytosis of HIV Gag. *AIDS Rev* 2007; **9**: 150–161.
14 Urano E, Aoki T, Futahashi Y, Murakami T, Morikawa Y, Yamamoto N *et al.* Substitution of the myristoylation signal of human immunodeficiency virus type 1 Pr55Gag with the phospholipase C-delta1 pleckstrin homology domain results in infectious pseudovirion production. *J Gen Virol* 2008; **89**: 3144–3149.
15 Garrus JE, von Schwedler UK, Pornillos OW, Morham SG, Zavitz KH, Wang HE *et al.* Tsg101 and the vacuolar protein sorting pathway are essential for HIV-1 budding. *Cell* 2001; **107**: 55–65.
16 Lindwasser OW, Resh MD. Multimerization of human immunodeficiency virus type 1 Gag promotes its localization to barges, raft-like membrane microdomains. *J Virol* 2001; **75**: 7913–7924.
17 Ono A, Freed EO. Plasma membrane rafts play a critical role in HIV-1 assembly and release. *Proc Natl Acad Sci USA* 2001; **98**: 13925–13930.
18 Ono A, Freed EO. Binding of human immunodeficiency virus type 1 Gag to membrane: role of the matrix amino terminus. *J Virol* 1999; **73**: 4136–4144.
19 Gottlinger HG, Sodroski JG, Haseltine WA. Role of capsid precursor processing and myristoylation in morphogenesis and infectivity of human immunodeficiency virus type 1. *Proc Natl Acad Sci USA* 1989; **86**: 5781–5785.
20 Zhou W, Resh MD. Differential membrane binding of the human immunodeficiency virus type 1 matrix protein. *J Virol* 1996; **70**: 8540–8548.
21 Wagner R, Graf M, Bieler K, Wolf H, Grunwald T, Foley P *et al.* Rev-independent expression of synthetic gag-pol genes of human immunodeficiency virus type 1 and simian immunodeficiency virus: implications for the safety of lentiviral vectors. *Hum Gene Ther* 2000; **11**: 2403–2413.
22 Komano J, Miyauchi K, Matsuda Z, Yamamoto N. Inhibiting the Arp2/3 complex limits infection of both intracellular mature vaccinia virus and primate lentiviruses. *Mol Biol Cell* 2004; **15**: 5197–5207.
23 Gao F, Li Y, Decker JM, Peyerl FW, Bibollet-Ruche F, Rodenburg CM *et al.* Codon usage optimization of HIV type 1 subtype C gag, pol, env, and nef genes: *in vitro* expression and immune responses in DNA-vaccinated mice. *AIDS Res Hum Retroviruses* 2003; **19**: 817–823.
24 Stauffer TP, Ahn S, Meyer T. Receptor-induced transient reduction in plasma membrane PtdIns(4,5)P2 concentration monitored in living cells. *Curr Biol* 1998; **8**: 343–346.
25 Hamatake M, Aoki T, Futahashi Y, Urano E, Yamamoto N, Komano J. Ligand-independent higher-order multimerization of CXCR4, a G-protein-coupled chemokine receptor involved in targeted metastasis. *Cancer Sci* 2009; **100**: 95 .

Bioorganic & Medicinal Chemistry 19 (2011) 6735–6742

Contents lists available at SciVerse ScienceDirect

Bioorganic & Medicinal Chemistry

journal homepage: www.elsevier.com/locate/bmc

Small molecular CD4 mimics as HIV entry inhibitors

Tetsuo Narumi [a], Hiroshi Arai [a], Kazuhisa Yoshimura [b], Shigeyoshi Harada [b], Wataru Nomura [a], Shuzo Matsushita [b], Hirokazu Tamamura [a,*]

[a] Institute of Biomaterials and Bioengineering, Tokyo Medical and Dental University, Chiyoda-ku, Tokyo 101-0062, Japan
[b] Center for AIDS Research, Kumamoto University, Kumamoto 860-0811, Japan

ARTICLE INFO

Article history:
Received 5 August 2011
Revised 23 September 2011
Accepted 24 September 2011
Available online 29 September 2011

Keywords:
CD4 mimic
HIV entry
gp120-CD4 interaction
Phe43 cavity

ABSTRACT

Derivatives of CD4 mimics were designed and synthesized to interact with the conserved residues of the Phe43 cavity in gp120 to investigate their anti-HIV activity, cytotoxicity, and CD4 mimicry effects on conformational changes of gp120. Significant potency gains were made by installation of bulky hydrophobic groups into the piperidine moiety, resulting in discovery of a potent compound with a higher selective index and CD4 mimicry. The current study identified a novel lead compound **11** with significant anti-HIV activity and lower cytotoxicity than those of known CD4 mimics.

1. Introduction

The dynamic supramolecular mechanism of HIV cellular invasion has emerged as a key target for blocking HIV entry into host cells.[1] HIV entry begins with the interaction of a viral envelope glycoprotein gp120 and a cell surface protein CD4.[2] This triggers extensive conformational changes in gp120 exposing co-receptor binding domains and allowing the subsequent binding of gp120 to a co-receptor, CCR5[3]/CXCR4.[4] Following the viral attachment and co-receptor binding, gp41, another viral envelope glycoprotein mediates the fusion of the viral and cell membranes, thus completing the infection. Molecules interacting with each of these steps are potential candidates for anti-HIV-1 drugs. In particular, discovery and development of novel drugs that inhibit the viral attachment are required for blocking the HIV infection at an early stage.[5]

In 2005, small molecular CD4 mimics targeting the viral attachment were identified by an HIV syncytium formation assay and shown to bind within the Phe43 cavity, a highly conserved pocket on gp120,[6] which is a hydrophobic cavity occupied by the aromatic ring of Phe43 of CD4.[7] These molecules are comprised of three essential moieties: an aromatic ring, an oxalamide linker, and a piperidine ring (Fig. 1) and show micromolar order potency against diverse HIV-1 strains including laboratory and primary isolates. Furthermore, they possess the unique ability to induce the conformational changes in gp120 required for binding with soluble CD4.[8] Such CD4 mimicry can be an advantage for rendering the envelope more sensitive to neutralizing antibodies.[9] While such properties are promising for the development of HIV entry inhibitors and the use combinatorially with neutralizing antibodies, cytotoxicity is one of the drawbacks of CD4 mimics.

To date, we and others have performed structure–activity relationship (SAR) studies of CD4 mimics based on modifications of the aromatic ring, the oxalamide linker, and the piperidine moiety of CD4 mimics. In an initial survey of SAR studies of NBD-556 and NBD-557, Madani et al. revealed that potency (i.e., CD4 binding and mimicry) was highly sensitive to modifications of the aromatic ring, which is thought to bind in the Phe43 cavity of gp120 (Fig. 1). The CD4 mimic analogs (JRC-II-191) with a *para*-chloro-*meta*-fluorophenyl ring had significantly increased affinity for gp120.[10] Our SAR studies also revealed that a certain size and electron-withdrawing ability of the *para*-substituents are indispensable for potent anti-HIV activity.[11] Furthermore, the replacement of the chlorine group at the *para* position with a methyl group which is almost as bulky as a bromine atom leads to improvement of solubility of the compounds in buffer to provide the reproducibility in the biological studies with comparable biological activities.

Further SAR studies were focused on the piperidine moiety of CD4 mimics to investigate its contribution to biological activities, and we found that the piperidine ring is critical for the CD4 mimicry on the conformational changes in gp120 and that substituents on the nitrogen of the piperidine moiety can contribute significantly to both anti-HIV activity and cytotoxicity.[12] Based on these SARs and our modeling study, we speculate that interactions of the piperidine moiety with several amino acids in the vicinity of the Phe43 cavity in gp120, specifically an electrostatic interaction with

* Corresponding author. Tel.: +81 3 5280 8036; fax: +81 3 5280 8039.
E-mail address: tamamura.mr@tmd.ac.jp (H. Tamamura).

0968-0896/$ - see front matter © 2011 Elsevier Ltd. All rights reserved.
doi:10.1016/j.bmc.2011.09.045

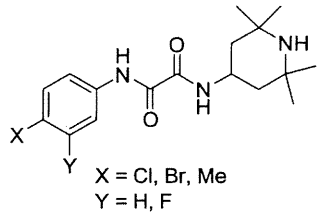

Figure 1. CD4 mimics.

Asp368 and a hydrophobic interaction with Val430, are critical for biological activity. LaLonde et al. focused on modifications of the piperidine moiety using computational approaches, adducing evidence for the importance of these interactions to the binding affinity against gp120.[13] Based on these results, we envisioned that an enhancement of the interaction of CD4 mimics with residues associated with the Phe43 cavity in gp120 would lead to the increase of their potency and CD4 mimicry inducing the conformational changes of gp120, and the decrease of their cytotoxicity. Thus, in this study a series of CD4 mimics, which were designed to interact with the conserved residues in the Phe43 cavity, were synthesized to increase binding affinity for gp120, and the appropriate SAR studies were performed.

2. Results and discussion

Two types of CD4 mimic analogs were designed: (1) CD4 mimics with the ability to interact electrostatically with Asp368, and (2) CD4 mimics with the ability to interact hydrophobically with Val430 (Fig. 2). The X-ray structure of gp120 bound to soluble CD4 (PDB: 1RZJ) revealed that the guanidino group of Arg59 of CD4 is involved in a hydrogen bond with Asp368 of gp120. In order to mimic this interaction, a guanidino and related groups such as thiourea and urea were introduced to the piperidine moiety of the CD4 mimic derivative COC-021, which was developed in order to modify the nitrogen of the piperidine moiety and which showed biological activity, including anti-HIV activity and CD4 mimicry, similar to that of the parent compound NBD-556.[12] Furthermore, to interact with Val430 by hydrophobic interaction, the methyl groups on the piperidine ring were replaced with cyclohexyl groups to prepare a novel CD4 mimic analog with enhanced hydrophobicity.

2.1. Chemistry

The syntheses of CD4 mimics are outlined in Scheme 1. CD4 mimics with guanidine, thiourea, and urea groups on the piperidine moiety were prepared using our previously reported method.[12] Coupling of *p*-chloroaniline with ethyl chloroglyoxylate followed by aminolysis of the ethyl ester with 4-amino-*N*-benzylpiperidine under microwave conditions (150 °C, 3 h) gave the corresponding amide. Removal of the benzyl group with 1-chloroethyl chloroformate[14] gave the free piperidine moiety, which was modified to produce the desired compounds **4**–**8** (Scheme 1).

For synthesis of a CD4 mimic derivative with two cyclohexyl groups, treatment of 2,2,6,6-tetramethylpiperidin-4-one **9** with cyclohexanone in the presence of ammonium chloride furnished a 2,6-substituted piperidin-4-one derivative,[15] and reductive amination with benzylamine and subsequent removal of benzyl group provided a primary amine **10**. Microwave-assisted aminolysis of ester **2** with amine **10** yielded the desired dicyclohexyl-substituted analog **11** (Scheme 2). The synthesis of the other compounds is described in Supplementary data.

2.2. Biological studies

The anti-HIV activity of synthetic CD4 mimics was evaluated in a single-round viral infective assay. Inhibition of HIV-1 infection was measured as reduction in β-galactosidase gene expression after a single-round of virus infection of TZM-bl cells as described previously.[9] IC_{50} was defined as the concentration that caused a 50% reduction in the β-galactosidase activity (relative light units [RLU]) compared to virus control wells. Cytotoxicity

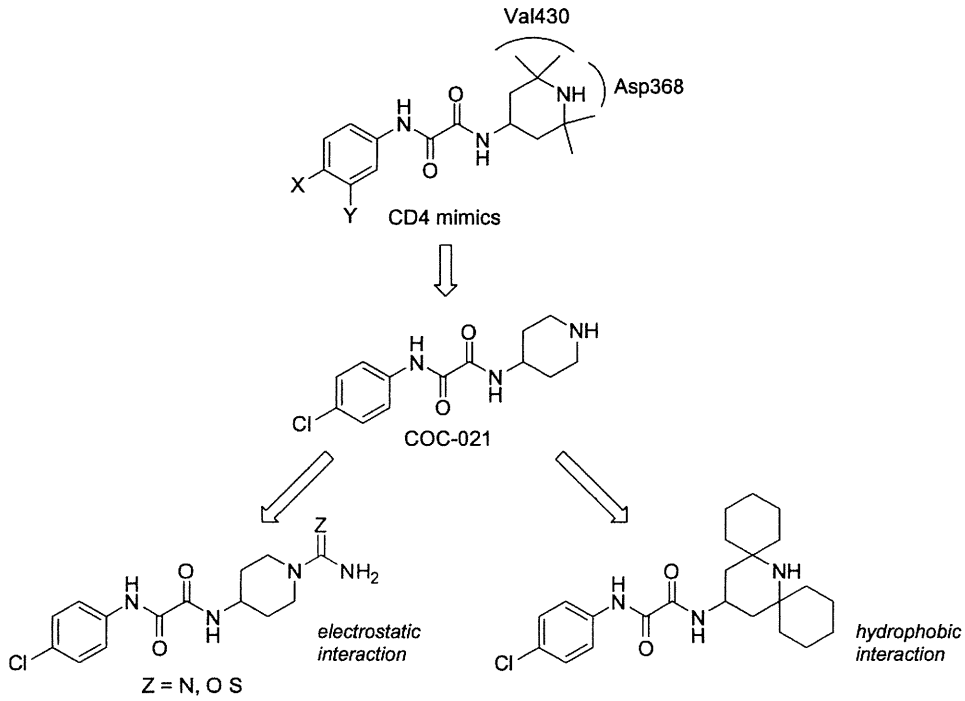

Figure 2. Design strategy for novel CD4 mimics with enhanced electrostatic/hydrophobic interaction.

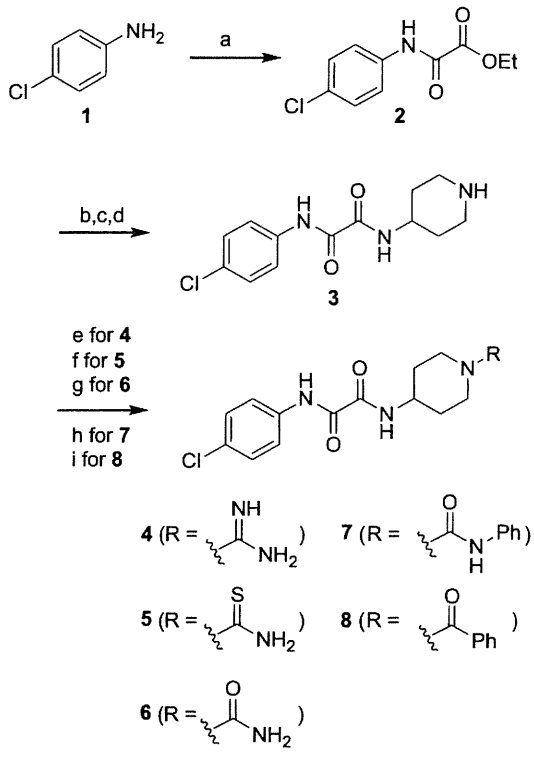

Scheme 1. Synthesis of N-modified piperidine derivatives **4–8**. Reagents and conditions: (a) Ethyl chloroglyoxylate, Et_3N, THF, quant.; (b) 1-benzyl-4-aminopiperidine, Et_3N, EtOH, 150 °C, microwave, 78%; (c) 1-chloroethyl chloroformate, CH_2Cl_2; (d) MeOH, reflux, 64% in two steps; (e) 1*H*-pyrazole-1-carboxamidine hydrochloride, Et_3N, DMF, 61%; (f) (trimethylsilyl)isothiocyanate, $CHCl_3$, 36%; (g) (trimethylsilyl)isocyanate, $CHCl_3$, 30%; (h) phenyl isocyanate, $CHCl_3$, 32%, (i) benzoyl chloride, Et_3N, CH_2Cl_2, 68%.

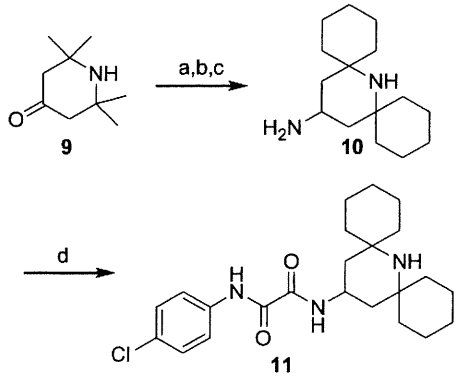

Scheme 2. Synthesis of dicyclohexyl derivative **11**. Reagents and conditions: (a) Cyclohexanone, NH_4Cl, DMSO, 60 °C; (b) benzylamine, $NaBH_4$, MeOH; (c) 10% Pd/C, H_2, MeOH, 7% from **9**; (d) **2**, Et_3N, EtOH, 150 °C, microwave, 17%.

of the compounds based on the viability of mock-infected PM1/CCR5 cells was evaluated using WST-8 method. The assay results for the CD4 mimics **3–8** are shown in Table 1. Compound **12** (NBD-556) showed potent anti-HIV activity; its IC_{50} value was 0.61 μM, and it is thus 13–20-fold more potent than the reported values.[11,12] Although previous studies found that compound **13**, with a methyl group at the *p*-position of the phenyl ring, and compound **3**, with no dimethyl groups on the piperidine ring, showed potent anti-HIV activity, only moderate activities were observed in the current study; this is about 12–14-fold less potency than reported for compound **12** and is probably due to

Table 1
Effects of the nitrogen-substituents on anti-HIV activity and cytotoxicity of CD4 mimic analogs[a]

Compd	X	R	IC_{50}[b] (μM)	CC_{50}[c] (μM)	SI (CC_{50}/IC_{50})
			YTA (R5)		
3[d]	Cl	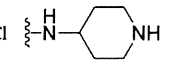	7.0	51	7.3
4[e]	Cl	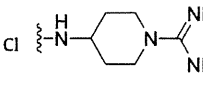	6.1	72	12
5	Cl	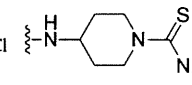	5.5	42	7.6
6	Cl	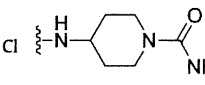	8.3	310	37
7	Cl	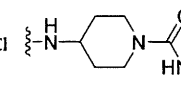	11	6.2	0.56
8	Cl	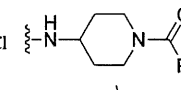	5.1	ND	–
12 (NBD-556)	Cl	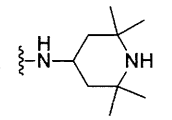	0.61	35	57
13	Me	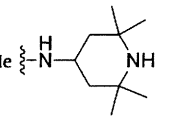	8.4	260	31

[a] All data with standard deviation are the mean values for at least three independent experiments (ND = not determined)
[b] IC_{50} values are based on the reduction in the β-galactosidase activity in TZM-bl cells.
[c] CC_{50} values are based on the reduction of the viability of mock-infected PM1/CCR5 cells.
[d] Desalted by satd $NaHCO_3$ aq.
[e] TFA salts.

the different assay system. All of the synthesized novel derivatives of compound **12** showed moderate to potent anti-HIV activity. A guanidine derivative **4** and thiourea derivative **5** showed potent anti-HIV activities (IC_{50} of **4** = 6.1 μM and IC_{50} of **5** = 5.5 μM) but their potency was approximately 10-fold lower than that of the parent compound **12**. A urea derivative **6** also showed potent anti-HIV activity (IC_{50} = 8.3 μM) and exhibited lower cytotoxicity (CC_{50} = 310 μM). On the other hand, introduction of a phenyl group in the urea derivative **6**, led to an *N*-phenylurea derivative **7**, with an increase of cytotoxicity (CC_{50} = 6.2 μM). To examine the influence of the N–H group on anti-HIV activity, an *N*-benzoyl derivative **8** was also tested. The IC_{50} value of **8** was 5.1 μM, which is equipotent with the thioamide derivative **5**. The *N*-benzoyl derivative **8** was essentially equipotent with **3** and this result suggests the presence of the hydrogen atom of the N–H group does not contribute to an increase in anti-HIV activity. The thiourea derivative **5** and the *N*-phenylurea derivative **7**, which have more acidic protons (pK_a of thiourea and *N*-phenylurea; 21.0 and 19.5,[16] respectively) than the urea derivative **6** (pK_a of urea; 26.9[16]), were found to exhibit relatively strong cytotoxicity. This observation indicates that

Table 2
Anti-HIV activity and cytotoxicity of CD4 mimic analogs **11**, **12**, and **14–17**[a]

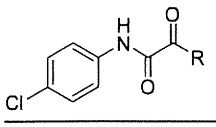

Compd	R	IC_{50}[b] (μM)	CC_{50}[c] (μM)	SI (CC_{50}/IC_{50})
		YTA (R5)		
11	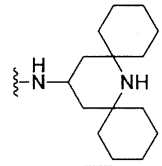	0.68	120	176
14	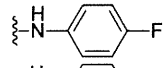	3.1	>500	>160
15	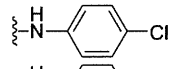	>100	>500	–
16	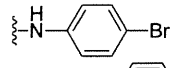	>100	>500	–
17	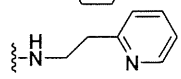	19.8	480	24
12 (NBD-556)	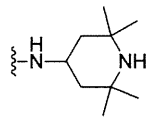	0.61	35	57

[a] All data with standard deviation are the mean values for at least three independent experiments
[b] IC_{50} values are based on the reduction in the β-galactosidase activity in TZM-bl cells.
[c] CC_{50} values are based on the reduction of the viability of mock-infected PM1/CCR5 cells.

Table 3
Anti-HIV activity of CD4 mimic **12** and dicyclohexyl derivative **11**[a]

Compd	R	IC_{50}[b] (μM) Single-round assay	IC_{50}[c] (μM) Multi-round assay
12 (NBD-556)	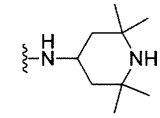	0.61	0.90
11	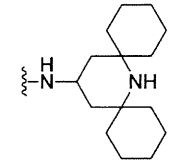	0.68	0.56

[a] All data with standard deviation are the mean values for at least three independent experiments.
[b] IC_{50} values of the single-round assay are based on the reduction in the β-galactosidase activity in TZM-bl cells.
[c] IC_{50} values of the multi-round assay are based on the inhibition of HIV-1-induced cytopathogenicity in PM1/CCR5 cells.

substitution on the piperidine moiety of acidic functional groups was unfavorable.

The assay results for CD4 mimics that target hydrophobic interactions are shown in Table 2. Compound **11** showed significant anti-HIV activity (IC_{50} = 0.68 μM) comparable to that of the lead compound **12**, but exhibited lower cytotoxicity. Compound **11** showed approximately four-fold less cytotoxicity than **12**. The SI of **11** is 176, 3 times higher than that of **12** (SI = 57). This result suggests that substitution of bulky hydrophobic groups into the piperidine moiety may be consistent with lower cytotoxicity of CD4 mimics. It is noteworthy that compound **14**, which has a *p*-fluoroanilino group in place of the piperidine ring, exhibits potent anti-HIV activity (IC_{50} = 3.1 μM) without significant cytotoxicity (CC_{50} >500 μM). The SI of compound **14** is >160, which is comparable to that of **11**. However, replacement of the piperidine moiety with a *p*-bromo- or *p*-chloroanilino group resulted in the loss of anti-HIV activity. These results suggest that the introduction of a fluorine atom to the piperidine moiety might be consistent with improvement of the anti-HIV activity. Extension of the alkyl chain by two carbons, as in **17** resulted in a 30-fold loss of anti-HIV activity, indicating that relatively rigid structures are preferable for anti-HIV activity.

The anti-HIV activities of **12** and compound **11**, which has a higher SI than the parent compound **12** were evaluated in a multi-round viral infective assay and the results are shown in Table 3. In this assay, the IC_{50} value of **12** was 0.90 μM, which was slightly larger value than measured in a single-round assay (IC_{50} = 0.61 μM). Compound **11** showed higher anti-HIV activity (IC_{50} = 0.56 μM) than compound **12**, indicating that the introduction of hydrophobic cyclohexyl groups into the piperdine moiety has a positive effect on not only the cytotoxicity but also the anti-HIV activity. This is possibly due to the stability in the assay condition derived from the hydrophobicity of cyclohexyl group(s). These results are consistent with a previous study of the analog with one hydrophobic *gem*-dimethyl group on the piperidine moiety, a compound with potent anti-HIV activity and efficient binding affinity for gp120.[13]

To gain insight into the interactions involved in the binding, molecular modeling of compound **11** docked into gp120 (1RZJ) was carried with Sybyl 7.1 (Fig. 3). The binding mode of compound **11** in the Phe43 cavity suggested that the orientation of the piperidine moiety of **11** is different from that in compound **12**, and that the cyclohexyl group can be positioned near Val430 with whose isopropyl group it can interact hydrophobically.

Fluorescence activated cell sorting (FACS) analysis was performed as previously reported,[11,12] to evaluate the CD4 mimicry effects on conformational changes of gp120 and the results are shown in Figure 4. Comparison of the binding of an anti-envelope CD4-induced monoclonal antibody (4C11) to the cell surface pretreated with the above CD4 mimics was measured in terms of the mean fluorescence intensity (MFI). Our previous studies revealed that the profile of the binding of 4C11 to the Env-expressing cell surface pretreated with compound **12** was entirely similar to that of pretreatment of soluble CD4. In this FACS analysis, the MFI of pretreatment with compound **12** is 23.13. The profiles of the binding of 4C11 to the cell surface pretreated with compounds **3**, **4** and **5** were comparable to that of compound **12** [MFI (**3**) = 20.54, MFI (**4**) = 20.85, MFI (**5**) = 20.24, respectively], suggesting that these derivatives offer a significant enhancement of binding affinity for 4C11. On the other hand, pretreatment with **6** and **8** did not cause significant enhancement of the binding affinity for 4C11, indicating that introduction of a carbonyl group on the piperidine nitrogen is not conducive to CD4 mimicry. The profile of the binding of 4C11 to the Env-expressing cell surface pretreated with compound **11**, which had significant anti-HIV activity and lower cytotoxicity than compound **12**, (MFI (**11**) = 22.17) was similar to that of compound **12**, suggesting that compound **11** offers significant enhancement of binding affinity for 4C11. This result indicates that compound **11** retains the CD4 mimicry on the conformational changes of gp120. Although compound **14** and compound **17** showed potent anti-HIV activity and no significant cytotoxicity, the profiles pretreated with (MFI (**14** and **17**) = 15.20 and 15.38) were similar to that of the control (MFI = 14.94), suggesting that these compounds **14** and **17** failed to produce a significant increase in binding affinity for 4C11. These

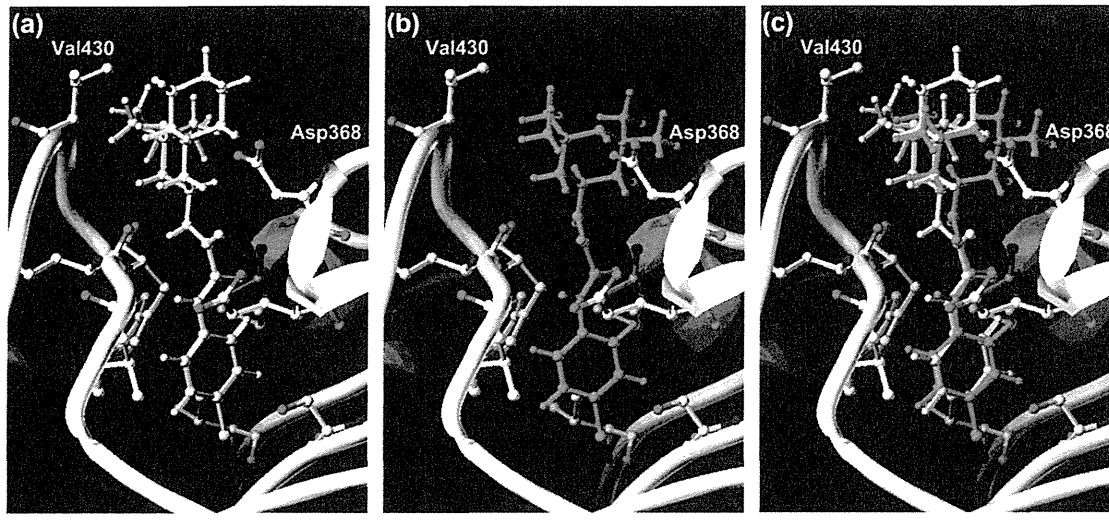

Figure 3. Docking structures of (a) compound **11** and (b) compound **12** bound in the Phe43 cavity of gp120 (1RZJ); (c) merge image of compounds **11** and **12**. Compounds **11** and **12** are represented in yellow and green sticks, respectively. Key residues in the cavity forming interactions with compounds are represented in gray sticks.

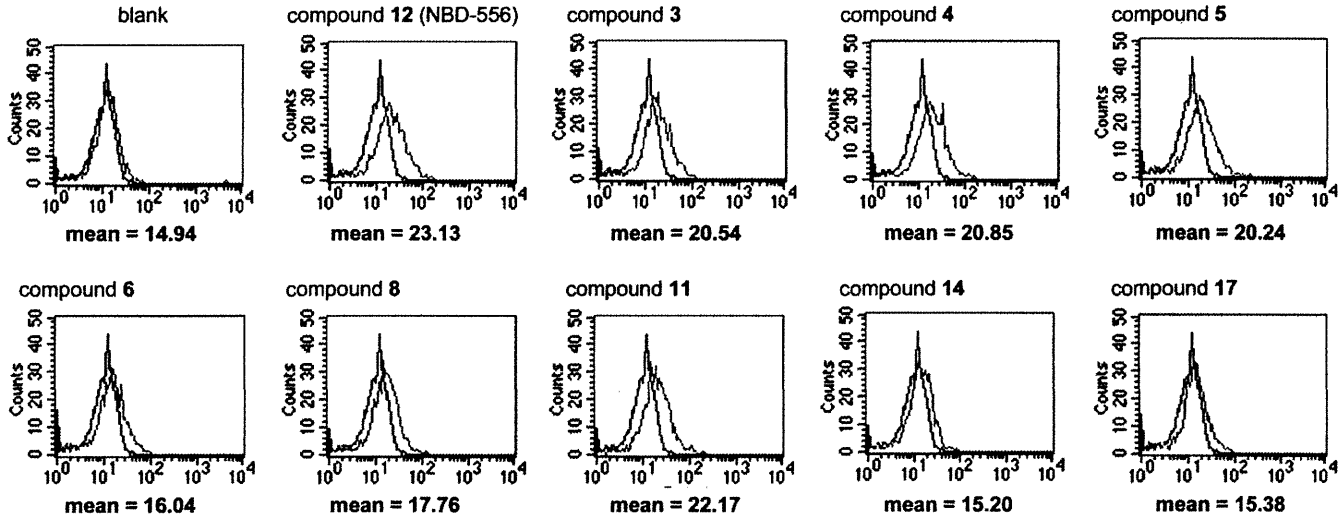

Figure 4. FACS analysis of compounds **12**, **3–6**, **8** (Table 1), **11**, **14**, and **17** (Table 2).

results are consistent with our previous finding that the piperidine ring is critical to the CD4 mimicry of the conformational changes in gp120.

3. Conclusion

A series of CD4 mimics were designed and synthesized to interact with the conserved residues in the Phe43 cavity of gp120 to investigate their anti-HIV activity, cytotoxicity, and CD4 mimicry as a function of conformational change of gp120. The biological activities of the synthetic compounds indicate that (1) the hydrogen atom of the piperidine moieties contributes significantly to cytotoxicity, and (2) installation of bulky hydrophobic groups into the piperidine moiety can increase anti-HIV activity and decrease cytotoxicity thus providing a novel compound with higher selective index than those of the original CD4 mimics. Furthermore, this modification has no great influence on the CD4 mimicry on the conformational change of gp120. Thus, compound **11** is promising for further studies. More detailed SAR investigations with respect to the substitution on the piperidine moiety have been ongoing studies.

4. Experimentals

^{1}H NMR and ^{13}C NMR spectra were recorded using a Bruker Avance III spectrometer. Chemical shifts are reported in δ (ppm) relative to Me_4Si (in $CDCl_3$) as internal standard. Low- and high-resolution mass spectra were recorded on a Bruker Daltonics microTOF focus in the positive and negative detection mode. For flash chromatography, Wakogel C-200 (Wako Pure Chemical Industries, Ltd) and silica gel 60 N (Kanto Chemical Co., Inc.) were employed. For analytical HPLC, a Cosmosil 5C_{18}-ARII column (4.6 × 250 mm, Nacalai Tesque, Inc., Kyoto, Japan) was employed with a linear gradient of CH_3CN containing 0.1% (v/v) TFA at a flow rate of 1 cm^3 min^{-1} on a JASCO PU-2089 plus (JASCO Corporation, Ltd., Tokyo, Japan), and eluting products were detected by UV at 220 nm. Preparative HPLC was performed using a Cosmosil 5C_{18}-ARII column (20 × 250 mm, Nacalai Tesque, Inc.) on a JASCO PU-2087 plus (JASCO Corporation, Ltd, Tokyo, Japan) in a suitable

gradient mode of CH_3CN solution containing 0.1% (v/v) TFA at a flow rate of 7 cm^3 min^{-1}. Microwave reactions were performed in Biotage Microwave Reaction Kit (sealed vials) in an Initiator™ (Biotage). The wattage was automatically adjusted to maintain the desired temperature for the desired period of time.

4.1. Chemistry

4.1.1. N^1-(4-Chlorophenyl)-N^2-(piperidin-4-yl)oxalamide (3)

To a stirred solution of *p*-choroaniline (**1**) (14.0 g, 110 mmol) in THF (146 mL) were added ethyl chloroglyoxylate (8.13 mL, 73.2 mmol) and triethylamine (Et_3N) (15.2 mL, 110 mmol) at 0 °C. The mixture was stirred for 6 h at room temperature. After the precipitate was filtrated off, the filtrate solution was concentrated under reduced pressure. The residue was dissolve in EtOAc, and washed with 1 M HCl, saturated $NaHCO_3$ and brine, then dried over $MgSO_4$. Concentration under reduced pressure gave the crude ethyl oxalamate, which was used without further purification. To a solution of the above ethyl oxalamate (1.27 g, 5.25 mmol) in EtOH (13.0 mL) were added Et_3N (1.46 mL, 10.5 mmol) and 4-amino-1-benzylpiperidine (2.97 mL, 15.8 mmol). The reaction mixture was stirred for 3 h at 150 °C under microwave irradiation. After being cooled to room temperature, the crystal was collected and washed with cold EtOH and *n*-hexane, and dried under reduced pressure to provide the corresponding amide (1.58 g, 81% yield) as colorless crystals. To a stirred solution of **S1** (1.46 g, 3.90 mmol) in CH_2Cl_2 (39.0 mL) was added dropwise 1-chloroethyl chloroformate (0.860 mL, 7.80 mmol) at 0 °C. After being stirred at room temperature for 30 min, the mixture was refluxed for 1 h. After concentration under reduced pressure, the residue was dissolved in MeOH and then refluxed for 1 h. After concentration under reduced pressure, the residue was diluted with EtOAc and washed with saturated $NaHCO_3$ and brine, then dried over $MgSO_4$. After concentration under reduced pressure, the residue was washed with cold EtOAc, and dried under reduced pressure to provide the title compound **3** (778 mg, 71% yield) as white powder.

^1H NMR (400 MHz, $CDCl_3$) δ 1.39–1.52 (m, 2H), 1.92–2.01 (m, 2H), 2.67–2.79 (m, 2H), 3.06–3.19 (m, 2H), 3.83–3.95 (m, 1H), 7.34 (d, J = 8.80 Hz, 2H), 7.44 (d, J = 7.64 Hz, 1H), 7.59 (d, J = 8.80 Hz, 2H), 9.28 (s, 1H); ^{13}C NMR (125 MHz, $CDCl_3$) δ 33.0 (2C), 45.2 (2C), 47.9, 21.0 (2C), 129.3 (2C), 130.5, 135.0, 157.6, 158.8; HRMS (ESI), *m/z* calcd for $C_{13}H_{17}ClN_3O_2$ (MH^+) 282.1004, found 282.1002.

4.1.2. N^1-(1-Carbamimidoylpiperidin-4-yl)-N^2-(4-chlorophenyl) oxalamide (4)

To a stirred solution of **3** (50.0 mg, 0.178 mmol) in DMF (20.0 mL) was added 1-aminopyrazole hydrochlride (312 mg, 2.13 mmol) and Et_3N (0.390 mL, 28.1 mmol). The reaction mixture was stirred at room temperature for 24 h. After concentration under reduced pressure, purification by preparative HPLC gave the trifluoroacetate of the title compound **4** as white powder (36.0 mg, 61% yield).

^1H NMR (500 MHz, DMSO) δ 1.41–1.55 (m, 2H), 1.59–1.71 (m, 2H), 2.70–2.74 (m, 2H), 3.74–3.87 (m, 1H), 3.88–4.03 (m, 2H), 5.93 (s, 2H), 7.42 (d, J = 9.00 Hz, 2H), 7.85 (d, J = 9.00 Hz, 2H), 8.95 (d, J = 9.00 Hz, 1H), 10.80 (s, 1H); ^{13}C NMR (125 MHz, DMSO) δ 31.3 (2C), 43.0 (2C), 47.6, 122.4 (2C), 128.6, 129.1 (2C), 137.1, 158.2, 159.3, 159.5; HRMS (ESI), *m/z* calcd for $C_{14}H_{19}ClN_5O_2$ (MH^+) 324.1222, found 324.1213.

4.1.3. N^1-(1-Carbamothioylpiperidin-4-yl)-N^2-(4-chlorophenyl) oxalamide (5)

To a stirred solution of **3** (140 mg, 0.498 mmol) in $CHCl_3$ (5.00 mL) was added trimethylsilyl isothiocyanate (141 mL, 1.00 mmol) and stirred at room temperature for 1 h. The precipitate was collected and washed with cold $CHCl_3$, and dried under reduced pressure to provide the title compound **5** as white powder. (62.0 mg, 36% yield).

^1H NMR (400 MHz, DMSO) δ 1.45–1.69 (m, 2H), 1.69–1.81 (m, 2H), 2.67–2.81 (m, 2H), 3.02–3.16 (m, 2H), 3.75–3.89 (m, 1H), 7.41 (d, J = 9.00 Hz, 2H), 7.85 (d, J = 9.00 Hz, 2H), 9.00 (d, J = 8.50 Hz, 1H), 10.80 (s, 1H); ^{13}C NMR (125 MHz, DMSO) δ 27.8 (2C), 42.3 (2C), 44.4, 122.0 (2C), 128.2, 128.6 (2C), 129.5, 136.6, 158.6, 159.4; Anal. calcd for $C_{14}H_{18}ClN_4O_2S$: C, 49.34; H, 5.03; N, 16.44. Found: C, 49.32; H, 4.76; N, 16.11.

4.1.4. N^1-(1-Carbamoylpiperidin-4-yl)-N^2-(4-chlorophenyl) oxalamide (6)

To a stirred solution of **3** (60.0 mg, 0.213 mmol) in $CHCl_3$ (1.10 mL) was added trimethylsilyl isocyanate (56.0 μL, 0.421 mmol), and the mixture was stirred at room temperature for 1 h. The precipitate was collected and washed with cold $CHCl_3$, and dried under reduced pressure to provide the title compound **6** (20.1 mg, 30% yield) as white powder.

^1H NMR (500 MHz, DMSO) δ 1.44–1.55 (m, 2H), 1.58–1.71 (m, 2H), 2.65–2.78 (m, 2H), 3.76–3.87 (m, 1H), 3.87–4.01 (m, 2H), 5.94 (s, 1H), 7.42 (d, J = 9.00 Hz, 2H), 7.86 (d, J = 9.00 Hz, 2H), 8.95 (d, J = 9.00 Hz, 1H), 10.80 (s, 1H); ^{13}C NMR (125 MHz, DMSO) δ 30.8 (2C), 42.6 (2C), 47.1, 122.0 (2C), 128.1, 128.6 (2C), 136.7, 157.8, 158.8, 159.0; HRMS (ESI), *m/z* calcd for $C_{14}H_{18}ClN_4O_3$ (MH^+) 325.1062, found 325.1060.

4.1.5. N^1-(4-Chlorophenyl)-N^2-(1-(phenylcarbamoyl)piperidin-4-yl)oxalamide (7)

To a stirred solution of **3** (140 mg, 0.498 mmol) in $CHCl_3$ (5.00 mL) was added phenyl isocyanate (54.0 μL, 0.500 mmol) and stirred at room temperature for 1 h. The precipitate was collected and washed with cold $CHCl_3$, and dried under reduced pressure to provide the title compound **7** as white powder. (64.1 mg, 32% yield).

^1H NMR (500 MHz, DMSO) δ 1.52–1.66 (m, 2H), 1.68–1.80 (m, 2H), 2.81–2.95 (m, 2H), 3.84–3.96 (m, 1H), 4.08–4.20 (m, 2H), 6.91–6.94 (m, 2H), 7.21–7.24 (m, 2H), 7.36–7.52 (m, 4H), 7.86 (d, J = 9.00 Hz, 2H), 8.53 (s, 1H), 8.99 (d, J = 8.50 Hz, 2H), 10.81 (s, 1H); ^{13}C NMR (125 MHz, DMSO) δ 31.3 (2C), 43.4 (2C), 47.5, 120.0 (2C), 122.0, 122.4 (2C), 128.6, 128.7 (2C), 129.1 (2C), 137.1, 141.1, 155.2, 159.2, 159.5; HRMS (ESI), *m/z* calcd for $C_{20}H_{22}ClN_4O_3$ (MH^+) 401.1375, found 401.1372.

4.1.6. N^1-(1-Benzoylpiperidin-4-yl)-N^2-(4-chlorophenyl) oxalamide (8)

To a stirred solution of **3** (500 mg, 1.78 mmol) in $CHCl_3$ (17.8 mL) was added benzoyl chloride (307 μL, 2.67 mmol) and the mixture was stirred at room temperature for 1 h. The precipitate was collected and washed with cold EtOAc, and dried under reduced pressure to provide the title compound **8** (232 mg, 34% yield).

^1H NMR (500 MHz, $CDCl_3$) δ 1.21–1.68 (br, 4H), 1.96–2.08 (br, 2H), 3.02–3.16 (br, 2H), 4.04–4.07 (m, 1H), 7.35 (d, J = 9.00 Hz, 2H), 7.41–7.43 (m, 5H), 7.52 (d, J = 8.00 Hz, 1H), 7.59 (d, J = 9.00 Hz, 2H), 9.25 (s, 1H); ^{13}C NMR (125 MHz, $CDCl_3$) δ 31.4 (2C), 41.0 (2C), 47.6, 121.0 (2C), 126.9 (2C), 128.6 (2C), 129.3 (2C), 129.9, 130.6, 134.8, 135.6, 157.2, 159.0, 170.5; HRMS (ESI), *m/z* calcd for $C_{20}H_{21}ClN_3O_3$ (MH^+) 386.1266, found 386.1276.

4.1.7. Amine (10)

To a stirred solution of 2,2,6,6-tetramethylpiperidin-4-one (7.75 g, 50.0 mmol) and cyclohexanone (15.5 mL, 150 mmol) in DMSO (71.0 mL) was added NH_4Cl (16.1 g, 300 mmol) and stirred at 60 °C for 5 h. The reaction mixture was diluted with H_2O

(150 mL), acidified with 7% aq HCl, and extracted with Et_2O (200 mL × 3). The water layer was adjusted to pH 9 using 10% aq K_2CO_3 and then back-extracted with EtOAc. The extract was washed with brine and dried over Na_2SO_4. After concentration under reduced pressure, the residue was dissolve in MeOH (60.0 mL) and benzylamine (10.9 mL, 100 mmol) was added. After being stirred at room temperature for 1 h, sodium cyanoborohydride was added and stirred at room temperature for 6 h. The reaction mixture was poured into saturated $NaHCO_3$ and extracted with EtOAc, then dried over $MgSO_4$. After concentration under reduced pressure, the residue was dissolve in MeOH (150 mL) and 10% Pd/C (5.32 g, 5.00 mmol) was added and stirred at room temperature for 24 h under hydrogen atmosphere. After the reaction mixture was filtered through celite, the filtrate solution was concentrated under reduced pressure followed by flash chromatography over silica gel with EtOAc–EtOH (4:1) to gave the title compound **10** (820 mg, 7 % yield) as a colorless oil.

^{1}H NMR (500 MHz, $CDCl_3$) δ 0.730 (t, J = 12.0 Hz, 2H), 1.15–1.85 (m, 23H), 2.01–3.7 (m, 2H), 2.95–3.05 (m, 1H); ^{13}C NMR (125 MHz, $CDCl_3$) δ 22.2 (2C), 22.8 (2C), 26.2 (2C), 37.3 (2C), 42.3 (2C), 43.6 (2C), 47.0, 53.2 (2C); HRMS (ESI), m/z calcd for $C_{15}H_{29}N_2$ (MH^+) 237.2325, found 237.2321.

4.1.8. N^1-(4-Chlorophenyl)-N^2-(2,6-dicyclohexylpiperidin-4-yl) oxalamide (11)

To a solution of **10** (722 mg, 3.05 mmol) in EtOH (15.0 mL) was added ethyl 2-((4-chlorophenyl)amino)-2-oxoacetate (363 mg, 1.50 mmol) and triethylamine (0.415 mL, 3.00 mmol) and stirred for 3 h at 150 °C under microwave irradiation. The mixture was filtered and the precipitate was collected and washed with cold EtOH, and dried under reduced pressure to provide the compound **11** (108 mg, 17% yield) as white powder.

^{1}H NMR (500 MHz, DMSO) δ 1.12–1.91 (br, 24H), 4.02–4.07 (m, 1H), 7.42 (d, J = 9.00 Hz, 2H), 7.84 (d, J = 9.00 Hz, 2H), 8.76 (br, 1H), 9.25 (s, 1H); ^{13}C NMR (125 MHz, $CDCl_3$) δ 22.1 (2C), 22.7 (2C), 26.0 (2C), 37.2 (2C), 42.5 (2C), 42.9 (2C), 43.6, 52.7 (2C), 120.9 (2C), 129.3 (2C), 130.4, 135.0, 157.6, 158.8; HRMS (ESI), m/z calcd for $C_{23}H_{33}ClN_3O_2$ (MH^+) 418.2256, found 418.2261.

4.1.9. N^1-(4-Chlorophenyl)-N^2-(4-fluorophenyl)oxalamide (14)

To a solution of the ethyl 2-((4-chlorophenyl)amino)-2-oxoacetate (1.21 g, 5.00 mmol) in EtOH (25.0 mL) were added Et_3N (1.38 mL, 10.0 mmol) and 4-fluoroaniline **12** (1.44 mL, 15.0 mmol). The reaction mixture was stirred for 3 h at 150 °C under microwave irradiation. After being cooled to room temperature, the crystal was collected and washed with cold EtOH and n-hexane, and dried under reduced pressure to provide the compound **14** (601 mg, 41% yield) as colorless crystals. Compounds **15** and **16** were similarly synthesized.

^{1}H NMR (500 MHz, $CDCl_3$) δ 7.07–7.14 (m, 2H), 7.35–7.40 (m, 2H), 7.59–7.63 (m, 4H), 9.29 (s, 1H), 9.33 (s, 1H); ^{13}C NMR (125 MHz, DMSO) δ 115.8 (d, J = 22.5 Hz, 2C), 122.5 (2C), 122.8 (d, J = 7.5 Hz, 2C), 128.8, 129.1 (2C), 134.4, 137.1, 158.3, 158.9 (d, J = 42.5 Hz), 160.2; HRMS (ESI), m/z calcd for $C_{14}H_{11}ClFN_2O_2$ (MH^+) 293.0488, found 293.0485.

4.1.10. N^1-(4-Chlorophenyl)-N^2-(2-(pyridin-2-yl)ethyl) oxalamide (17)

To a solution of the ethyl 2-((4-chlorophenyl)amino)-2-oxoacetate (726.3 mg, 3.00 mmol) in EtOH (10.0 mL) were added Et_3N (0.831 mL, 6.00 mmol) and 2-(pyridin-2-yl)ethanamine 14 (1.07 mL, 9.00 mmol). The reaction mixture was stirred for 3 h at 150 °C under microwave irradiation. After being cooled to room temperature, the crystal was collected and washed with cold EtOH and n-hexane, and dried under reduced pressure to provide the title compound **17** (336 mg, 37% yield) as colorless crystals.

^{1}H NMR (500 MHz, $CDCl_3$) δ 3.08 (t, J = 6.50 Hz, 2H), 3.82 (q, J = 6.50 Hz, 2H), 7.12–7.21 (m, 2H), 7.30–7.37 (m, 2H),7.54–7.66 (m 3H), 8.40 (s, 1H), 8.60 (d, J = 5.00 Hz, 1H), 9.26 (s, 1H); ^{13}C NMR (125 MHz, $CDCl_3$) δ 36.5, 39.0, 121.0 (2C), 121.8, 123.4, 129.2 (2C), 130.3, 135.1, 136.7, 149.5, 157.5, 158.6, 159.6; HRMS (ESI), m/z calcd for $C_{15}H_{15}ClN_3O_2$ (MH^+) 304.0847, found 304.0850.

4.2. Molecular modeling

The structures of compounds **11** and **12** were built in Sybyl and minimized with the MMFF94 force field and partial charges.[17] Dockings were then performed using FlexSIS through its SYBYL module, into the crystal structure of gp120 (PDB: 1RZJ).

4.3. FACS analysis

JR-FL (R5, Sub B) chronically infected PM1 cells were pre-incubated with 100 μM of a CD4 mimic for 15 min, and then incubated with an anti-HIV-1 mAb, 4C11, at 4 °C for 15 min. The cells were washed with PBS, and fluorescein isothiocyanate (FITC)-conjugated goat anti-human IgG antibody was used for antibody-staining. Flow cytometry data for the binding of 4C11 (green lines, Fig. 4) to the Env-expressing cell surface in the presence of a CD4 mimic are shown among gated PM1 cells along with a control antibody (anti-human CD19: black lines, Fig. 4). Data are representative of the results from a minimum of two independent experiments. The number at the bottom of each graph in Figure 4 shows the mean fluorescence intensity (MFI) of the antibody 4C11.

Acknowledgments

This work was supported in part by Grant-in-Aid for Scientific Research from the Ministry of Education, Culture, Sports, Science, and Technology of Japan, and Health and Labour Sciences Research Grants from Japanese Ministry of Health, Labor, and Welfare.

Supplementary data

Supplementary data (NMR charts of compounds) associated with this article can be found, in the online version, at doi:10.1016/j.bmc.2011.09.045.

References and notes

1. Selected reviews of the drug developments targeting HIV entry process: (a) Blair, W. S.; Lin, P. F.; Meanwell, N. A.; Wallace, O. B. *Drug Discovery Today* **2000**, *5*, 183; (b) D'Souza, M. P.; Cairns, J. S.; Plaeger, S. F. *J. Am. Med. Assoc.* **2000**, *284*, 215; (c) Labranche, C. C.; Galasso, G.; Moore, J. P.; Bolognesi, D.; Hirsch, M. S.; Hammer, S. M. *Antivir. Res.* **2001**, *50*, 95; (d) Pierson, T. C.; Doms, R. W. *Immunol. Lett.* **2003**, *85*, 113; (e) Tamamura, H.; Otaka, A.; Fujii, N. *Curr. HIV Res.* **2005**, *3*, 289.
2. Chan, D. C.; Kim, P. S. *Cell* **1998**, *93*, 681.
3. (a) Alkhatib, G.; Combadiere, C.; Broder, C. C.; Feng, Y.; Kennedy, P. E.; Murphy, P. M.; Berger, E. A. *Science* **1996**, *272*, 1955; (b) Choe, H.; Farzan, M.; Sun, Y.; Sullivan, N.; Rollins, B.; Ponath, P. D.; Wu, L.; Mackay, C. R.; LaRosa, G.; Newman, W.; Gerard, N.; Gerard, C.; Sodroski, J. *Cell* **1996**, *85*, 1135; (c) Deng, H. K.; Liu, R.; Ellmeier, W.; Choe, S.; Unutmaz, D.; Burkhart, M.; Marzio, P. D.; Marmon, S.; Sutton, R. E.; Hill, C. M.; Davis, C. B.; Peiper, S. C.; Schall, T. J.; Littman, D. R.; Landau, N. R. *Nature* **1996**, *381*, 661; (d) Doranz, B. J.; Rucker, J.; Yi, Y. J.; Smyth, R. J.; Samson, M.; Peiper, S. C.; Parmentier, M.; Collman, R. G.; Doms, R. W. *Cell* **1996**, *85*, 1149; (e) Dragic, T.; Litwin, V.; Allaway, G. P.; Martin, S. R.; Huang, Y.; Nagashima, K. A.; Cayanan, C.; Maddon, P. J.; Koup, R. A.; Moore, J. P.; Paxton, W. A. *Nature* **1996**, *381*, 667.
4. Feng, Y.; Broder, C. C.; Kennedy, P. E.; Berger, E. A. *Science* **1996**, *272*, 872.
5. (a) Briz, V.; Poveda, E.; Soriano, V. *J. Antimicrob. Chemother.* **2006**, *57*, 619; (b) Rusconi, S.; Scozzafava, A.; Mastrolorenzo, A.; Supuran, C. T. *Curr. Drug Targets Infect. Disord.* **2004**, *4*, 339; (c) Shaheen, F.; Collman, R. G. *Curr. Opin. Infect. Dis.* **2004**, *17*, 7; (d) Markovic, I. *Curr. Pharm. Des.* **2006**, *12*, 1105.
6. Zhao, Q.; Ma, L.; Jiang, S.; Lu, H.; Liu, S.; He, Y.; Strick, N.; Neamati, N.; Debnath, A. K. *Virology* **2005**, *339*, 213.
7. (a) Kwong, P. D.; Wyatt, R.; Robinson, J.; Sweet, R. W.; Sodroski, J.; Hendrickson, W. A. *Nature* **1998**, *393*, 648; (b) Kwong, P. D.; Wyatt, R.; Mcajeed, S.; Robinson, J.; Sweet, R. W.; Sodroski, J.; Hendrickson, W. A. *Structure* **2000**, *8*, 1329.

8. Schön, A.; Madani, N.; Klein, J. C.; Hubicki, A.; Ng, D.; Yang, X.; Smith, A. B., III; Sodroski, J.; Freire, E. *Biochemistry* **2006**, *45*, 10973.
9. Yoshimura, K.; Harada, S.; Shibata, J.; Hatada, M.; Yamada, Y.; Ochiai, C.; Tamamura, H.; Matsushita, S. *J. Virol.* **2010**, *84*, 7558.
10. Madani, N.; Schön, A.; Princiotto, A. M.; LaLonde, J. M.; Courter, J. R.; Soeta, T.; Ng, D.; Wang, L.; Brower, E. T.; Xiang, S.-H.; Do Kwon, Y.; Huang, C.-C.; Wyatt, R.; Kwong, P. D.; Freire, E.; Smith, A. B., III; Sodroski, J. *Structure* **2008**, *16*, 1689.
11. Yamada, Y.; Ochiai, C.; Yoshimura, K.; Tanaka, T.; Ohashi, N.; Narumi, T.; Nomura, W.; Harada, S.; Matsushita, S.; Tamamura, H. *Bioorg. Med. Chem. Lett.* **2010**, *20*, 354.
12. Narumi, T.; Ochiai, C.; Yoshimura, K.; Harada, S.; Tanaka, T.; Nomura, W.; Arai, H.; Ozaki, T.; Ohashi, N.; Matsushita, S.; Tamamura, H. *Bioorg. Med. Chem. Lett.* **2010**, *20*, 5853.
13. LaLonde, J. M.; Elban, M. A.; Courter, J. R.; Sugawara, A.; Soeta, T.; Madani, N.; Princiotto, A. M.; Kwon, Y. D.; Kwong, P. D.; Schön, A.; Freire, E.; Sodroski, J.; Smith, A. B., III *Bioorg. Med. Chem. Lett.* **2011**, *20*, 354.
14. Olofson, R. A.; Abbott, D. E. *J. Org. Chem.* **1984**, *49*, 2795.
15. Sakai, K.; Yamada, K.; Yamasaki, T.; Kinoshita, Y.; Mito, F.; Utsumi, H. *Tetrahedron* **2010**, *66*, 2311.
16. Bordwell, F. G.; Ji, G. Z. *J. Am. Chem. Soc.* **1991**, *113*, 8398.
17. Halgren, T. A. *J. Comput. Chem.* **1996**, *17*, 490.

DOI: 10.1002/cbic.201000670

Synthetic Caged DAG-lactones for Photochemically Controlled Activation of Protein Kinase C

Wataru Nomura,[a] Tetsuo Narumi,[a] Nami Ohashi,[a] Yuki Serizawa,[a] Nancy E. Lewin,[b] Peter M. Blumberg,[b] Toshiaki Furuta,[a, c] and Hirokazu Tamamura*[a]

The signal transduction pathways associated with interactions with small organic molecules attract great interest in the field of chemical biology. To study the action of bioactive compounds in detail, it is necessary to eliminate the signaling complexity caused by multiple combined effects. The development of "caged" compounds, which are not active when the pharmacophore is blocked by a photoactivatable moiety, has been a powerful tool with which to approach this problem. Triggered by photoirradiation to a limited area in the cell, the specific effects of the ligand in that location can then be observed over time. Several strategies for "caging" molecules have been developed and each approach has its own advantages.[1]

The protein kinase C (PKC) isoforms play pivotal roles in physiological responses to growth factors and oxidative stress mediated through the endogenous second messenger 1,2-diacylglycerol (DAG). These responses regulate numerous cellular processes,[2] including proliferation,[3] differentiation,[4] migration,[5] and apoptosis.[6] The tumor-promoting phorbol esters, potent analogues of DAG, have provided a convenient probe of PKC function. Ligand binding to the C1b domain in PKC leads to its membrane translocation. The translocation of PKC is of central importance for its function because the localization of PKC determines the substrates to which it has access.[7] Despite the complex regulatory mechanisms of PKC activation, considerable progress in understanding isozyme-specific functions has been made.[8] Development of ligands with high specificities for PKC isozymes has been a critical issue in the medicinal field.[9a-b] Enhancement of the understanding of targets and signaling pathways would provide important insights contributing to this effort.

As high-affinity ligands for PKC, DAG-lactones have established the importance of the pharmacophore triad of two carbonyl groups (*sn*-1 and *sn*-2) and the hydroxy group being maintained intact.[8] In this study, we have utilized coumarin-based "caging" molecules including 6-bromo-7-hydroxycoumarin (Bhc)[10] and 6-bromo-7-methoxycoumarin (Bmc)[11] to block the binding of DAG-lactones to PKCδ. The caged protecting groups are attached to the primary alcohol, which is an important DAG-lactone pharmacophore. Photolytic uncaging of the blocked DAG-lactone then provides a means of driving PKC activation within the cell at desired specific locations and times. An approach previously used to achieve this goal has been the use of caged diacylglycerols.[1d,12] DAG-lactones have several potential advantages. Extensive medical chemistry investigations have yielded DAG-lactones with substantially enhanced affinities, a range of physiochemical properties, and interesting biological selectivities with regard to diacylglycerol targets.[8]

The DAG-lactones have been developed as ligands for PKC isozymes with low-nanomolar binding affinities by a combination of pharmacophore- and receptor-guided approaches based on the structure of the physiological second messenger DAG (Scheme 1).[8] The DAG-lactones were designed by the

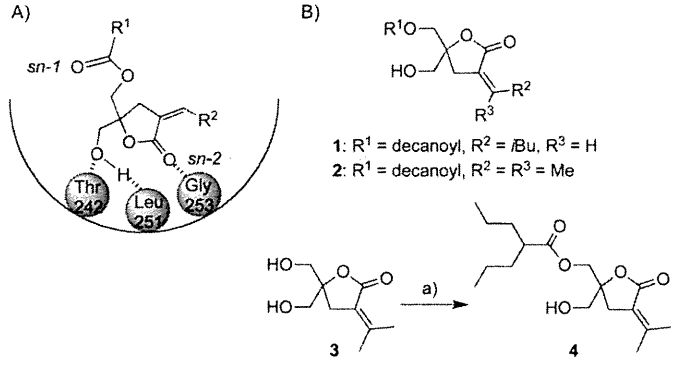

Scheme 1. A) The *sn*-2 binding model of DAG-lactones to the PKCδ C1b domain and membrane. B) Structures of the DAG-lactones **1**, **2**, and **4**. a) 2-Propylpentanoyl chloride, pyridine, CH_2Cl_2, 24%.

pharmacophore-guided approach based on the geometries of bioequivalent pharmacophores present in DAG and in phorbol esters.[13] In the DAG-lactone structure, the glycerol backbone was constrained to a γ-lactone ring to reduce the entropic penalty associated with DAG binding. In binding to PKC, the linear or branched acyl (R^1) or α-alkylidene (R^2) chains contribute to optimized hydrophobic interactions with a group of conserved hydrophobic amino acids located on the top half of the C1 domain. There are two competing binding modes (*sn*-1 and *sn*-2), depending on which carbonyl group is directly involved in binding to the protein (Scheme 1A). In general, it

[a] *Dr. W. Nomura, Dr. T. Narumi, N. Ohashi, Y. Serizawa, Prof. T. Furuta, Prof. H. Tamamura*
Department of Medicinal Chemistry
Institute of Biomaterials and Bioengineering
Tokyo Medical and Dental University
2-3-10 Kandasurugadai, Chiyoda-ku, Tokyo 101-0062 (Japan)
Fax:(+81) 3-5280-8039
E-mail: tamamura.mr@tmd.ac.jp

[b] *N. E. Lewin, Dr. P. M. Blumberg*
Laboratory of Cancer Biology and Genetics, Center for Cancer Research
National Cancer Institute, National Institutes of Health
Bethesda, Maryland 20892 (USA)

[c] *Prof. T. Furuta*
Faculty of Science, Toho University
2-2-1 Miyama, Funabashi, Chiba 274-8510 (Japan)

Supporting information for this article is available on the WWW under http://dx.doi.org/10.1002/cbic.201000670.

has been found that DAG favors *sn*-1 binding, whereas the corresponding DAG-lactone analogues favor *sn*-2 binding.[8] In this study, three representative DAG-lactones—**1**, **2**, and **4** (Scheme 1B)—were investigated. Compound **1** had previously been reported as part of a branched α-alkylidene series that provided the most potent α-alkylidene analogues.[9,14] Comparison of the binding affinities of the stereoisomers showed that the *Z* isomer of lactone **1** had a higher affinity for PKCδ than the *E* isomer. The *Z* isomer of compound **1** was therefore purified by flash chromatography and utilized for experiments. Compound **2** had also previously been synthesized to assess the role of a flexible decanoic acid chain at the acyl chain position (R^1).[9a] Compound **4** was synthesized as a compound with a branched chain as an acyloxy moiety and an isopropyl system as an α-alkylidene group; a similar compound with a more branched acyloxy moiety has been reported.[15] The lactones **2** and **4** each contain an isopropylidene group at the α-alkylidene position, which has been identified as one of the principal determinants for control of biological activity. The effect of the acyl group on the isozyme specificity of the DAG-lactones has been investigated with a series of compounds.

The binding affinities of the DAG-lactones were determined as described previously.[16] The K_i values of the compounds were determined as 8.4 ± 2.9, 6.5 ± 0.8, and 22 ± 1.6 nM (mean ± SEM) for **1**, **2**, and **4**, respectively. The binding affinities of **1** and **2** were compatible with those in the previous reports[9a,15b] (2.3 and 15.9 nM, respectively), whereas that of **4** was weaker than those of the related compounds. It has been reported that branched chains interfere with the interaction with the hydrophobic surface of the C1b domain in the *sn*-2 binding mode of DAG-lactones. As reported previously, the acyl and α-alkylidene moieties affect PKCδ translocation caused by ligand binding. To reveal the translocation caused by the synthesized DAG-lactones, CHO-K1 cells expressing a PKCδ-EGFP fusion construct were prepared and the PKCδ-EGFP was visualized by confocal microscopy as a function of time after ligand addition (Figure 1A–C). Compound **1** at 10 μM did not cause translocation of PKCδ even 30 min after addition (data not shown). Compound **2** caused rapid translocation, requiring 5 min for complete translocation. Compound **4** caused less complete and slower translocation, perhaps reflecting its weaker potency. As described for other DAG-lactones, translocation was predominantly to internal membrane compartments (nuclear membrane, mitochondria, and other cellular organelles).[17] From these studies, compound **2** was selected as the most suitable for photoactivation analysis with the aid of caged protecting groups.

To study PKCδ activation by photolysis of ligands, caged compounds were synthesized as depicted in Scheme 1B. As caging moieties, (6-bromo-7-hydroxycoumarin-4-yl)methoxycarbonyl (Bhcmoc) and (6-bromo-7-methoxycoumarin-4-yl)methoxycarbonyl (Bmcmoc) were utilized. Several caged compounds based on these caging moieties have been reported previously.[1c] As one of the most commonly used classes of structures for the protection of phosphate, amine, and carbonyl functional groups, coumarin-based protecting groups including MCM,[18] HCM (and ACM),[19] DMCM,[20] BCMCM,[21] DMACM (and DEACM),[22] and Bhc[10] have been successfully developed. Given its critical role in forming two of the three hydrogen bonds driving binding of the DAG-lactone to the binding pocket of the C1 domain, the hydroxy group of the DAG-lactone was the obvious site for addition of the coumarin-based protecting group in order to disrupt binding (Scheme 1A).

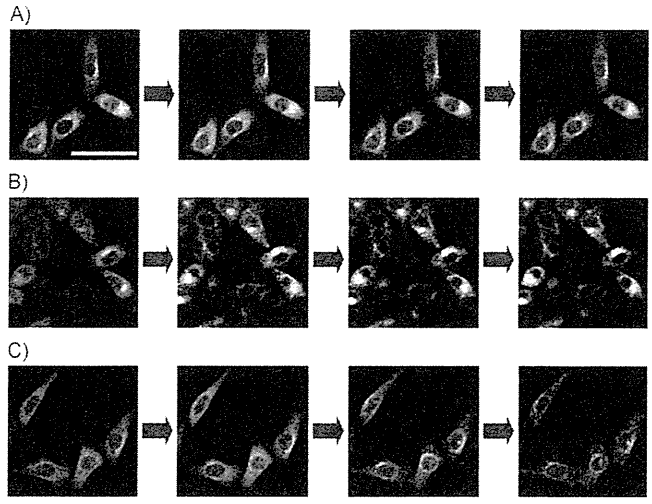

Figure 1. Translocation of PKCδ caused by compounds **1**, **2**, and **4**. A)–C) Time-dependent translocation of compounds **1**, **2**, and **4**, respectively (0, 1, 5, and 10 min after addition of compounds). The final concentration of the compounds was 10 μM. The scale bar indicates 50 μm.

The function of the Bhc- and Bmc-protected DAG-lactones **10** and **11** as "phototriggers" (Figure 2A) was evaluated in terms of several parameters. Firstly, the UV spectra of the compounds were determined (Figure 2B). The compounds showed clear absorbance originating from the caged moiety. The absorbance maxima for Bhc-**2** and Bmc-**2** were 377 and 329 nm, respectively. Next, photolysis was performed with the aid of a photochemical lamp (RPR3500 Å). The breakdown of the caged compounds and the production of the uncaged compounds were monitored by HPLC and the extent of the reaction was calculated from the peak areas, which were determined as a function of irradiation time (Figure 2C). Quantitative production of the parent compound **2** was successfully observed. The preferred environment of the caging groups for photolysis is thus hydrophilic, accounting for the superiority of the Bhc group over the Bmc group in photolysis efficiency (Table S1 in the Supporting Information). The photochemical properties of Bmc-**1** and Bmc-**4** were also assessed. The results support the view that compound **2** is suitable for photoactivation analysis (Figures S1, S2, and Table S2).

To evaluate the binding affinities of the caged compounds, competitive binding analysis to PKCδ was performed as described previously.[16] The results indicated that the caged compounds, in which the hydroxy group was protected, showed decreases in binding affinity of more than 100-fold (Table S1). The measured binding affinities of Bhc-**2** (**10**) and Bmc-**2** (**11**) to PKCδ were 431 and 940 nM, respectively. For comparison, compound **2** without the blocking group had an affinity of 6.5 nM. In the proposed binding mode of the DAG-lactones to

